NATIONAL ADVISORY COMMITTEE FOR AERONAUTICS

TECHNICAL NOTE 2898

THEORETICAL CALCULATION OF THE PRESSURE DISTRIBUTION, SPAN LOADING, AND ROLLING MOMENT DUE TO SIDESLIP AT SUPERSONIC SPEEDS FOR THIN SWEPTBACK TAPERED WINGS WITH SUPERSONIC TRAILING EDGES AND WING TIPS PARALLEL TO THE AXIS OF WING SYMMETRY

By Kenneth Margolis, Windsor L. Sherman,
and Margery E. Hannah

Langley Aeronautical Laboratory
Langley Field, Va.

NACA

Washington
February 1953

NATIONAL ADVISORY COMMITTEE FOR AERONAUTICS

TECHNICAL NOTE 2898

THEORETICAL CALCULATION OF THE PRESSURE DISTRIBUTION, SPAN LOADING, AND ROLLING MOMENT DUE TO SIDESLIP AT SUPERSONIC SPEEDS FOR THIN SWEPTBACK TAPERED WINGS WITH SUPERSONIC TRAILING EDGES AND WING TIPS PARALLEL TO THE AXIS OF WING SYMMETRY

By Kenneth Margolis, Windsor L. Sherman,
and Margery E. Hannah

SUMMARY

On the basis of linearized supersonic-flow theory, an analysis was undertaken to determine the pressure distribution, span loading, and rolling moment due to small angles of sideslip at supersonic speeds for a series of thin, sweptback, tapered wings with wing tips parallel to the axis of wing symmetry. Three basic series of Mach number and plan-form combinations are considered, all of which have supersonic trailing edges in conjunction with one of the following: (a) both leading edges subsonic, (b) one leading edge subsonic and one leading edge supersonic, and (c) both leading edges supersonic. In addition to the Mach number limitation resulting from the supersonic-trailing-edge condition, the tip Mach lines may not intersect on the wing.

Results obtained for the configuration with both leading edges subsonic include formulas for the pressure distribution, span loading, rolling moment, and the corresponding stability derivative C_{l_β}. For configurations with a supersonic leading edge, formulas for the pressure distribution are presented.

Calculations covering a range of aspect ratio, taper ratio, Mach number, and leading-edge sweepback are presented for wings with both leading edges subsonic. All the wings treated showed negative values of C_{l_β} for positive angles of attack and positive values of C_{l_β} for negative angles of attack.

INTRODUCTION

A number of papers dealing with the theoretical calculations of stability derivatives for thin isolated wings at supersonic speeds have been published to date. Wing plan forms that have been treated in detail include the rectangular, trapezoidal, triangular, and modified forms of the triangular wing. (See, for example, refs. 1 to 10.) An important group of plan forms for which there are as yet incomplete data consists of the sweptback tapered wing with wing tips parallel to the axis of wing symmetry (usually termed "streamwise" tips for wings with zero sideslip). The lift-curve slope C_{L_α} is covered in detail in references 11 to 15; the damping-in-roll derivative C_{l_p} in references 11, 12, 16, and 17; the damping due to steady pitching (stability derivative C_{m_q}) in references 17 to 20; the pitching moment due to angle of attack (stability derivative C_{m_α}) in references 13, 18, and 20; the lift due to steady pitching (stability derivative C_{L_q}) in references 18 and 20. Some results for the lift and pitching-moment derivatives produced by constant vertical acceleration ($C_{L_{\dot{\alpha}}}$ and $C_{m_{\dot{\alpha}}}$) are presented in reference 21. References 22 and 23 treat the lateral force and yawing moment due to steady rolling (stability derivatives C_{Y_p} and C_{n_p}).

The present paper is primarily concerned with the rolling moment due to sideslip (stability derivative C_{l_β}). Reference 24 treats this derivative (and also the yawing-moment derivative C_{n_β}) by means of the conical-flow theory as previously utilized in references 13, 16, and 19 for other derivatives. The analysis given in reference 24 applies specifically to that family of plan forms for which all edges are subsonic, although the equations may also be applied to wings with subsonic leading edges and supersonic trailing edges. The development therein is quite complex and, as a result, calculations are presented for only two plan forms.

The combinations of wing plan form and Mach number considered herein all have supersonic trailing edges in conjunction with one of the following: (a) both leading edges subsonic, (b) one leading edge subsonic and one leading edge supersonic, and (c) both leading edges supersonic. A minor restriction (which, for practical configurations, materially limits the range of Mach numbers for very small aspect ratios only) is that the Mach lines emanating from the wing tips may not intersect on the wing.

For the configuration with both leading edges subsonic, an approximation based on Evvard's approach (ref. 25) for the tip region is utilized

in conjunction with conical-flow results for the remaining wing region. (See refs. 11 and 18 for analogous treatment of other wing motions.) Formulas for the pressure distribution, spanwise loading, and for the stability derivative C_{l_β} are derived as functions of wing geometry and Mach number. Numerical results are presented in the form of graphs showing illustrative spanwise loadings and the variation of the derivative C_{l_β} with Mach number for a range of aspect ratio, taper ratio, and leading-edge sweepback.

For configurations with a supersonic leading edge, expressions for the pressure distribution are derived for all wing regions by using Evvard's method (ref. 26).

SYMBOLS

V	free-stream velocity
M	free-stream Mach number, V/Speed of sound
μ	Mach angle
B	cotangent of Mach angle, $\sqrt{M^2 - 1}$
ρ	density of air
ΔP	local pressure difference between upper and lower surfaces of wing, positive in sense of lift
C_P	pressure coefficient, $\Delta P / \frac{1}{2}\rho V^2$
ϕ	perturbation velocity potential evaluated on upper surface of wing
c_y	wing chord at spanwise station y
b	wing span
c_r	wing root chord
λ	taper ratio, $\frac{\text{Tip chord}}{\text{Root chord}}$
A	aspect ratio, $\frac{b^2}{S} = \frac{2b}{c_r(1 + \lambda)}$

S wing area

n nondimensional spanwise coordinate, $\frac{y}{b/2}$

n_i value of n at spanwise station where tip Mach line from left half-wing intersects trailing edge of left half-wing,

$$\frac{\frac{4}{A(1+\lambda)} - \left[\frac{B}{m_1} + \frac{B^2 + m_3}{B(1 - m_3)}\right]}{\frac{B}{m_2} + \frac{B^2 + m_3}{B(1 - m_3)}}$$

n_j value of n at spanwise station where tip Mach line from right half-wing intersects trailing edge of right half-wing,

$$\frac{\left[\frac{B}{m_1} + \frac{B^2 - m_3}{B(1 + m_3)}\right] - \frac{4}{A(1+\lambda)}}{\frac{B}{m_2} + \frac{B^2 - m_3}{B(1 + m_3)}}$$

α angle of attack, radians

β angle of sideslip, positive as shown in figure 1, radians

ϵ angle between leading edge of wing and axis of wing symmetry (see fig. 1)

Λ leading-edge sweepback (see fig. 1)

δ angle between trailing edge of wing and axis of wing symmetry (see fig. 1)

$m_1 = B \tan \epsilon$

$m_2 = B \tan \delta$

$m_3 = B \tan \beta$

ω geometric parameter of wing, $\frac{2c_r \tan \epsilon}{b} = \frac{4m_1}{AB(1+\lambda)}$

S_W area of integration

$$k_1 = \frac{B \tan(\epsilon + \beta) - 1}{B \tan(\epsilon + \beta) + 1}$$

$$k_2 = \left| \frac{B \tan(\epsilon - \beta) + 1}{B \tan(\epsilon - \beta) - 1} \right|$$

$$k_3 = \frac{1 - B \tan \beta}{1 + B \tan \beta}$$

$$c = \frac{Mb}{2(\cos \beta + B \sin \beta)}$$

$$d = \frac{Mb}{2(\cos \beta - B \sin \beta)}$$

$P_0, P_1, \ldots P_4$ specific points used in appendixes

x, y rectangular coordinates (see fig. 1)

s, t rectangular coordinates (see fig. 3)

s', t' rectangular coordinates of source points

u, v oblique corrdinates (see fig. 5)

u_w, v_w oblique coordinates of field points

L' rolling moment

c_l airfoil-section lift coefficient, $\frac{1}{c_y}\int_{LE}^{TE} C_p \, dx$

C_l wing rolling-moment coefficient, $L' \Big/ \frac{1}{2}\rho V^2 Sb$

$$C_{l_\beta} = \left(\frac{\partial C_l}{\partial \beta} \right)_{\beta \to 0}$$

$E'(m_1)$ complete elliptic integral of second kind with modulus $\sqrt{1 - m_1^2}$, $\int_0^{\pi/2} \sqrt{1 - (1 - m_1^2)\sin^2 z}\, dz$

$$E''(m_1) = \frac{1}{E'(m_1)}$$

When the subscripts I, II, . . . XIV are used on a symbol, they indicate different wing regions. The symbols LE and TE refer to leading edge and trailing edge, respectively.

ANALYSIS

Scope

The general plan form considered in the present paper is sketched in figure 1; note that the wing tips are parallel to the axis of wing symmetry (usually referred to as streamwise tips for wings with zero sideslip). The analysis is subject to the usual restrictions and well-known limitations of the linearized supersonic-flow theory that are applicable to wings that have vanishingly small thickness and zero camber, that is, thin flat plates.

The range of Mach numbers considered permit the inclusion of all plan forms provided that the trailing edge is supersonic and that the tip Mach lines do not intersect on the wing. A general idea of the types of plan-form—Mach line configurations that are permitted may be obtained from figure 2. These configurations may be divided into three groups: (a) both leading edges subsonic, (b) one leading edge subsonic and one leading edge supersonic, and (c) both leading edges supersonic.

For the class of configurations with both leading edges subsonic, expressions are derived for the pressure distribution, span loading, rolling moment, and stability derivative C_{l_β}. Numerical results for the span loading and stability derivative are presented in graphical form. Inasmuch as further calculations may be desirable, it is useful to know the permissible range of geometric parameters and Mach number for which these aforementioned derivations are valid. When expressed explicitly as mathematical restrictions on the parameter $B \cot \Lambda$, the conditions of subsonic leading edges, supersonic trailing edges, and no tip Mach line intersections on the wing are given as follows:

$$\text{For } AB(1+\lambda) \geq \frac{\left[4(1+B\tan\beta)+A\tan\beta(1+\lambda)\right]\left[1-B\tan\beta-\tan\beta\cot\Lambda\right]}{2-\tan\beta\cot\Lambda},$$

$$\frac{AB(1+\lambda)(1+B\tan\beta)}{4(1-\lambda)(1+B\tan\beta)+A(1+\lambda)(B-\tan\beta)} \leqq B\cot\Lambda \leqq 1-B\tan\beta-\tan\beta\cot\Lambda$$

$$\text{For } AB(1+\lambda) < \frac{\left[4(1+B\tan\beta)+A\tan\beta(1+\lambda)\right]\left[1-B\tan\beta-\tan\beta\cot\Lambda\right]}{2-\tan\beta\cot\Lambda},$$

$$\frac{AB(1+\lambda)(1+B\tan\beta)}{4(1-\lambda)(1+B\tan\beta)+A(1+\lambda)(B-\tan\beta)} \leqq B\cot\Lambda \leqq \frac{AB(1+\lambda)(1+B\tan\beta)}{4(1+B\tan\beta)-A(1+\lambda)(B-\tan\beta)}$$

For the classes of configurations with one or both leading edges supersonic, expressions are derived for the pressure distribution.

All formulas and expressions for pressure distributions, span loadings, and moments are given in a body system of axes (see fig. 1). The resulting stability derivative C_{l_β} may be used directly in stability calculations without recourse to transfer terms inasmuch as the derivative has the same value in either body or stability systems of axes to the second order in α (the angle of attack).

General Considerations

The analysis is based on either exact or approximate solutions for the disturbance-velocity potential that satisfy the well-known requirements for linearized flow. (See ref. 11 for details regarding the approximation used.)

Consider a thin wing at an angle of attack in a sideslipping motion. The disturbance-velocity potential ϕ may be expressed relative to axes alined with the stream (usually referred to as wind axes) or with respect to axes that are fixed in the body (body axes). As indicated

in reference 4, for small angles of sideslip $\left(\beta \ll \frac{1}{M}\right)$ the linearized equation for the velocity potential has the same form relative to either system of axes. The potential expressed relative to wind axes is a function of the sideslip angle β, whereas the potential expressed relative to body axes is independent of sideslip. The distribution of lifting pressure ΔP is expressible in terms of the perturbation velocities evaluated on the upper wing surface as follows:

For wind axes (see fig. 3),

$$\Delta P = 2\rho V \frac{\partial \phi}{\partial s} \tag{1}$$

and the change in pressure distribution with sideslip results from the change in the potential function with sideslip.

For body axes and small sideslip (see fig. 3) the following approximate expression for ΔP is valid for wings or portions thereof that are swept behind the leading Mach cone and are not influenced by wing-tip or trailing-edge disturbances:

$$\Delta P = 2\rho V\left(\frac{\partial \phi}{\partial x} - \beta \frac{\partial \phi}{\partial y}\right) \tag{2}$$

The change in pressure distribution with sideslip results from the term $-\beta \frac{\partial \phi}{\partial y}$ since ϕ for this approximation is independent of sideslip. The expression for ϕ in this case is exactly that obtained for angle of attack in the absence of sideslip.

For the wing configuration with both leading edges subsonic, it has been found profitable to utilize both systems of axes in determining the pressure distribution. For the wings with one or both leading edges supersonic, the wind-axes system (eq. (1)) has been used exclusively to obtain the pressure distribution. After the pressure distribution is known, appropriate integrations will yield the spanwise-loading parameter

$$c_y c_l = \int_{LE}^{TE} C_P \, dx \tag{3}$$

and the rolling-moment coefficient

$$C_l = -\frac{1}{Sb}\int_{-b/2}^{b/2}\int_{LE}^{TE} C_{py}\, dx\, dy \tag{4}$$

The stability derivative C_{l_β} is then readily obtained:

$$C_{l_\beta} = \left(\frac{\partial C_l}{\partial \beta}\right)_{\beta \to 0} \tag{5}$$

Detailed Considerations

Wing with both leading edges subsonic.- For the configuration with both leading edges subsonic (see fig. 4), the wing is divided into three regions, one region external to the tip Mach cones (region I) and two tip regions (regions II and III). For small sideslip angles $\left(\beta \ll \frac{1}{M}\right)$, equation (2) is utilized to obtain the pressure distribution for region I. (Equation (1) is also applicable, but a simpler expression equally accurate to the first order in β is obtained by use of the body-axes system.) In the tip regions, the wind-axes system is used (eq. (1)). An approximation for the velocity potential (based on Evvard's method, ref. 25) which was previously used in reference 11 is modified to take into account the sideslip condition. Separate derivations are required for the two tip regions since the wing tip of region II acts as a leading edge whereas the wing tip of region III acts as a trailing edge. Thus, the pressure along the tip of region II becomes infinite, and the pressure along the tip of region III must be zero according to the Kutta-Joukowski hypothesis.

Expressions for the pressure distribution are derived in appendix A for these three regions. Figure 5 is to be used in conjunction with these derivations.

The pressure distributions have been analytically integrated to yield the span loading and the rolling moment. The stability derivative C_{l_β} has also been obtained. The resulting expressions are presented in appendix B. Values of the elliptic function $E''(m_1)$ (which appears in some of the equations) are obtainable from figure 6.

Wing with one leading edge subsonic and one leading edge supersonic.- The wing with one leading edge subsonic and one leading edge supersonic

is shown in figure 7. Derivations of the pressure distribution for wing regions IV to VIII are based on the method of reference 26 and are presented in appendix C. The pressure-distribution equation for region II, previously derived in appendix A, is also presented in appendix C (in the notation used for the supersonic-leading-edge configurations).

Wing with both leading edge supersonic.- Figure 8 presents the wing with both leading edges supersonic. Note that, although there are nine wing regions to be considered, there are only six regions remaining that require the derivation of pressures; the pressure distribution for regions IV, VI, and VIII have already been obtained in appendix C. The derivation of pressures for regions IX to XIV based on the method of reference 26 are carried out in appendix D.

It should be noted that configurations with other Mach line and plan-form combinations and with one or both leading edges supersonic are possible. All wing regions of such configurations, however, are merely duplicates of those already treated in appendixes C and D. (For example, see fig. 9.) Thus, the pressure distribution is obtained for these wings by choosing the appropriate formulas from appendixes C and D for the various wing regions.

DISCUSSION AND PRESENTATION OF RESULTS

The derivations given in appendixes A, C, and D enable the calculation of the pressure distribution due to small sideslip for a given wing provided the wing trailing edges are supersonic, the wing tips are parallel to the axis of wing symmetry, and the Mach lines from the two opposite side edges do not intersect on the wing. As has been previously indicated, there are 14 possible wing regions formed by Mach line and wing-edge boundaries each of which requires a separate derivation for the pressures. If the pressure distribution is desired for a given wing, the wing must first be subdivided into the various regions. (For example, see figs. 4, 7, 8, and 9.) The appropriate pressure-distribution equation must then be used to calculate the pressure in each region. For convenience, an index to these equations is given in table I.

The wing plan form with both leading edges subsonic has been treated in detail. The pressure distribution has been analytically integrated to yield the span loading and the rolling moment. Differentiation then yielded the stability derivative C_{l_β}. Based on the equations presented in appendix B, computations have been carried out for a number of plan forms at various Mach numbers.

Some illustrative variations of the span loading for $\beta = 0^\circ$, 2°, 5°, and 10° at Mach numbers of 1.2 and 1.5 are presented in figures 10 and 11. It will be noted that there is a more or less abrupt change in

slope at those spanwise stations where the tip Mach cones intersect the wing trailing edge. This discontinuity in slope is due to the abrupt change in pressures across the Mach cone boundary (see refs. 11 and 13).

Variations of the stability derivative C_{l_β} with Mach number are presented in figures 12 to 16 for families of wings of aspect ratio 2, 3, 4, 5, and 6. All the wings treated showed negative values of C_{l_β} for positive angles of attack and positive values of C_{l_β} for negative angles of attack.

CONCLUDING REMARKS

On the basis of linearized supersonic-flow theory, equations for the pressure distribution have been derived for thin, sweptback, tapered wings sideslipping at a constant angle of attack. The analysis is applicable to plan forms for which the wing tips are parallel to the axis of wing symmetry and at supersonic speeds for which the wing trailing edge is supersonic. A minor restriction is that the Mach cones emanating from the opposite side edges may not intersect on the wing.

The plan form with both leading edges subsonic has been analyzed in detail. Equations for the span loading, rolling moment, and the corresponding stability derivative C_{l_β} have been obtained. Illustrative span loadings and variations of the derivative C_{l_β} with Mach number are presented for a number of wings.

Langley Aeronautical Laboratory,
National Advisory Committee for Aeronautics,
Langley Field, Va., November 21, 1952.

APPENDIX A

DERIVATION OF EQUATIONS FOR THE PRESSURE DISTRIBUTION FOR WINGS WITH BOTH LEADING EDGES SUBSONIC

Equations are derived for the pressure distributions for wings with both leading edges subsonic. The plan form under consideration is shown in figure 4.

Region I.- As given by equation (2), the expression for ΔP for region I is

$$(\Delta P)_I = 2\rho V\left(\frac{\partial \phi_I}{\partial x} - \beta \frac{\partial \phi_I}{\partial y}\right) \tag{A1}$$

where ϕ_I is the velocity potential applicable to a wing at an angle of attack in the absence of sideslip. From reference 4, the velocity potential evaluated at the upper surface of the wing is

$$\phi_I = \frac{V\alpha\sqrt{x^2\tan^2\epsilon - y^2}}{E'(B \tan \epsilon)} \tag{A2}$$

The perturbation velocities $\frac{\partial \phi_I}{\partial x}$ and $\frac{\partial \phi_I}{\partial y}$ are then readily obtainable by differentiation

$$\frac{\partial \phi_I}{\partial x} = \frac{\alpha V \tan^2\epsilon}{E'(B \tan \epsilon)} \frac{x}{\sqrt{x^2\tan^2\epsilon - y^2}} \tag{A3}$$

and

$$\frac{\partial \phi_I}{\partial y} = \frac{\alpha V}{E'(B \tan \epsilon)} \frac{-y}{\sqrt{x^2\tan^2\epsilon - y^2}} \tag{A4}$$

Substitution of equations (A3) and (A4) into equation (A1) and division by $\frac{1}{2}\rho V^2$ yields the pressure-distribution equation in coefficient form:

$$(C_P)_I = \frac{(\Delta P)_I}{\frac{1}{2}\rho V^2} = \frac{4\alpha}{E'(B \tan \epsilon)} \frac{x \tan^2 \epsilon + \beta y}{\sqrt{x^2 \tan^2 \epsilon - y^2}} \tag{A5}$$

Region II.- It may be shown from references 25 and 11 that the velocity potential evaluated at the upper surface for a wing at a constant angle of attack may be approximated as

$$\phi(s,t) = \frac{V\alpha}{\pi} \iint_{S_W} \frac{ds'\, dt'}{\sqrt{(s - s')^2 - B^2(t - t')^2}} \tag{A6}$$

where S_W is a defined region of integration, s', t' are the rectangular coordinates of source points, and s, t are the rectangular coordinates of field points at which the potential is desired. The s- and t-axes (which correspond to the x- and y-axes used in refs. 25 and 26) are wind axes; the s-axis is alined with the free-stream velocity vector. Evvard (ref. 25) found it convenient to use on oblique u,v coordinate system in which lines of constant u and constant v are parallel to the Mach lines. The u,v system is related to the s',t' system as follows:

$$\left.\begin{aligned}
s' &= \frac{B}{M}(v + u) & v &= \frac{M}{2B}(s' + Bt') \\
t' &= \frac{1}{M}(v - u) & u &= \frac{M}{2B}(s' - Bt') \\
s &= \frac{B}{M}(v_w + u_w) & v_w &= \frac{M}{2B}(s + Bt) \\
t &= \frac{1}{M}(v_w - u_w) & u_w &= \frac{M}{2B}(s - Bt) \\
ds'\, dt' &= \frac{2B}{M^2}\, du\, dv
\end{aligned}\right\} \tag{A7}$$

In the u,v notation, equation (A6) becomes

$$\phi(u_w, v_w) = \frac{V\alpha}{\pi M} \iint_{S_W} \frac{du\, dv}{\sqrt{(u_w - u)(v_w - v)}} \tag{A8}$$

and, when applied specifically to region II, is

$$\phi_{II} = \frac{V\alpha}{M\pi} \int_{u_w/k_2}^{v_w} \frac{dv}{\sqrt{v_w - v}} \int_{k_3(v_w - d)}^{u_w} \frac{du}{\sqrt{u_w - u}} \tag{A9}$$

Information pertinent to the limits of integration and axes notation is given in figure 5.

Performing the integration indicated in equation (A9) yields

$$\phi_{II} = \frac{4V\alpha}{M\pi} \sqrt{u_w - k_3 v_w + k_3 d} \sqrt{v_w - \frac{u_w}{k_2}} \tag{A10}$$

Differentiation with respect to s may be carried out as follows:

$$\frac{\partial \phi_{II}}{\partial s} = \frac{\partial \phi_{II}}{\partial u_w} \frac{\partial u_w}{\partial s} + \frac{\partial \phi_{II}}{\partial v_w} \frac{\partial v_w}{\partial s} \tag{A11}$$

From equations (A7),

$$\left.\begin{aligned} \frac{\partial u_w}{\partial s} &= \frac{M}{2B} \\ \frac{\partial v_w}{\partial s} &= \frac{M}{2B} \end{aligned}\right\} \tag{A12}$$

and differentiation of equation (A10) leads to expressions for $\partial \phi_{II}/\partial u_w$ and $\partial \phi_{II}/\partial v_w$. After the indicated operations are performed and some

simplification is made, the following expression for $\partial\phi_{II}/\partial s$ results:

$$\frac{\partial\phi_{II}}{\partial s} = \frac{V\alpha}{\sqrt{k_2}\,\pi B}\left[(1 - k_3)\sqrt{\frac{k_2 v_w - u_w}{u_w - k_3 v_w + k_3 d}} + (k_2 - 1)\sqrt{\frac{u_w - k_3 v_w + k_3 d}{k_2 v_w - u_w}}\right] \tag{A13}$$

It is convenient to express equation (A13) in terms of the body-axes variables x and y and wing geometry. The variables u_w and v_w may be transformed into s and t by means of equations (A7). The variables s and t are in turn related to x and y by the rotation-of-axes formulas

$$\left.\begin{aligned} s &= x\cos\beta - y\sin\beta \\ t &= x\sin\beta + y\cos\beta \end{aligned}\right\} \tag{A14}$$

Combination of the two transformations given by equations (A7) and (A14) yields

$$\left.\begin{aligned} u_w &= \frac{M\cos\beta}{2B}\left[x(1 - B\tan\beta) - y(B + \tan\beta)\right] \\ v_w &= \frac{M\cos\beta}{2B}\left[x(1 + B\tan\beta) + y(B - \tan\beta)\right] \end{aligned}\right\} \tag{A15}$$

The constants k_2, k_3, and d are expressible as

$$\left.\begin{aligned} k_2 &= \left|\frac{B\tan(\epsilon - \beta) + 1}{B\tan(\epsilon - \beta) - 1}\right| \\ k_3 &= \frac{1 - B\tan\beta}{1 + B\tan\beta} \\ d &= \frac{Mb}{2(\cos\beta - B\sin\beta)} \end{aligned}\right\} \tag{A16}$$

It may be noted that, for all equations presented in both appendixes A and B and for all equations pertaining to wings with one leading edge subsonic, the constant k_2 may be written as

$$k_2 = \frac{1 + B \tan(\epsilon - \beta)}{1 - B \tan(\epsilon - \beta)}$$

When the relations given by equations (A15) and (A16) are used, the expression for $\partial\phi_{II}/\partial s$ given by equation (A13) may be rewritten as

$$\frac{\partial\phi_{II}}{\partial s} = \frac{V\alpha}{\pi\sqrt{1 + B \tan \beta}}\left[\frac{2 \tan \beta}{\sqrt{1 + B \tan(\epsilon - \beta)}}\sqrt{\frac{x \tan \epsilon + y}{(1 + \tan \epsilon \tan \beta)\left(\frac{b}{2} - y\right)}} + \frac{2 \tan(\epsilon - \beta)}{\sqrt{1 + B \tan(\epsilon - \beta)}}\sqrt{\frac{\left(\frac{b}{2} - y\right)(1 + \tan \epsilon \tan \beta)}{x \tan \epsilon + y}}\right] \tag{A17}$$

From equation (1),

$$(\Delta P)_{II} = 2\rho V \frac{\partial\phi_{II}}{\partial s}$$

or

$$(C_P)_{II} = \frac{4}{V} \frac{\partial\phi_{II}}{\partial s} \tag{A18}$$

Substitution of equation (A17) into equation (A18) yields

$$(C_P)_{II} = \frac{8\alpha}{\pi\sqrt{1 + B \tan \beta}\sqrt{1 + B \tan(\epsilon - \beta)}}\left[\tan \beta \sqrt{\frac{x \tan \epsilon + y}{\left(\frac{b}{2} - y\right)(1 + \tan \epsilon \tan \beta)}} + \tan(\epsilon - \beta)\sqrt{\frac{\left(\frac{b}{2} - y\right)(1 + \tan \epsilon \tan \beta)}{x \tan \epsilon + y}}\right] \tag{A19}$$

Region III.- The derivation of the pressure distribution for region III is analogous to that of region II with certain exceptions. The limits of integration for the potential are, of course, different (see fig. 5) and the Kutta-Joukowski condition is imposed on the velocity $\partial\phi/\partial s$ at the tip. (The tip of region III acts as a subsonic trailing edge whereas the tip of region II acts as a subsonic leading edge.)

Neglecting for a moment the flow conditions at the tip results in the following expression for the potential:

$$\phi_{III} = \frac{V\alpha}{M\pi} \int_{\frac{u_w - c}{k_3}}^{v_w} \frac{dv}{\sqrt{v_w - v}} \int_{-k_1 v_w}^{u_w} \frac{du}{\sqrt{u_w - u}} \tag{A20}$$

Performance of the integration indicated in equation (A20) yields

$$\phi_{III} = \frac{4V\alpha}{M\pi} \sqrt{u_w + k_1 v_w} \sqrt{\frac{k_3 v_w - u_w + c}{k_3}} \tag{A21}$$

Differentiation with respect to s (see eqs. (A11) and (A12)) yields

$$\frac{\partial \phi_{III}}{\partial s} = \frac{V\alpha}{\sqrt{k_3}\, B\pi} \left[(1 + k_1) \sqrt{\frac{k_3 v_w - u_w + c}{u_w + k_1 v_w}} + (k_3 - 1) \sqrt{\frac{u_w + k_1 v_w}{k_3 v_w - u_w + c}} \right] \tag{A22}$$

In order to satisfy the Kutta-Joukowski condition at the tip, $\left(\frac{\partial \phi_{III}}{\partial s}\right)_{Tip} = 0$. The first radical of the right-hand side of equation (A22) becomes zero at the tip whereas the second radical becomes infinite. Reference 26 shows that the proper solution is obtained by appropriate cancellation of the infinite velocity at the tip. The correct expression is given as

$$\frac{\partial \phi_{III}}{\partial s} = \frac{V\alpha}{\sqrt{k_3}\, B\pi} \left[(1 + k_1) \sqrt{\frac{k_3 v_w - u_w + c}{u_w + k_1 v_w}} \right] . \tag{A23}$$

Transformation to the x,y system yields

$$\frac{\partial \phi_{III}}{\partial s} = \frac{2V\alpha}{\pi} \frac{\tan(\epsilon + \beta)}{\sqrt{(1 - B \tan \beta)\left[B \tan(\epsilon + \beta) + 1\right]}} \sqrt{\frac{\left(y + \frac{b}{2}\right)(1 - \tan \epsilon \tan \beta)}{x \tan \epsilon - y}} \tag{A24}$$

where the parameters k_1 and c' have been replaced by

$$\left.\begin{aligned} k_1 &= \frac{B \tan(\epsilon + \beta) - 1}{B \tan(\epsilon + \beta) + 1} \\ c &= \frac{Mb}{2(\cos \beta + B \sin \beta)} \end{aligned}\right\} \tag{A25}$$

(See equations (A15) and (A16) for other pertinent substitutions.)

The pressure coefficient $\frac{4}{V} \frac{\partial \phi_{III}}{\partial s}$ is then obtained

$$(C_p)_{III} = \frac{8\alpha \tan(\epsilon + \beta)}{\pi \sqrt{\left[B \tan(\epsilon + \beta) + 1\right](1 - B \tan \beta)}} \sqrt{\frac{\left(y + \frac{b}{2}\right)(1 - \tan \epsilon \tan \beta)}{x \tan \epsilon - y}} \tag{A26}$$

APPENDIX B

FORMULAS FOR THE SPAN LOADING, ROLLING MOMENT, AND STABILITY DERIVATIVE C_{l_β} FOR WINGS WITH BOTH LEADING EDGES SUBSONIC

Formulas for the span loading, rolling moment, and the stability derivative C_{l_β} for wings with both leading edges subsonic are derived.

Span loading.- The pressure distributions given in appendix A have been integrated to yield the span loading parameter.

$$c_y c_l = \int_{LE}^{TE} C_p \, dx \tag{B1}$$

The following formulas result:

For $-1 \leq n < n_1$,

$$\frac{c_y c_l}{b\alpha} = 2\left[E''(m_1)\left(\sqrt{\left\{\left(\frac{m_1}{B}\right)\frac{B^2 + m_3}{B(1 - m_3)}(n + 1) + 1\right\}^2 - n^2} + \frac{m_3 n}{m_1}\cosh^{-1}\left|\frac{m_1}{Bn}\left[\frac{B^2 + m_3}{B(1 - m_3)}\right](n + 1) + \frac{1}{n}\right|\right) + \frac{4(m_1 + m_3)\sqrt{n + 1}}{\pi m_1\sqrt{\left(m_1 + m_3 + 1 - \frac{m_1 m_3}{B^2}\right)(1 - m_3)}}\left\{\sqrt{\frac{4m_1}{AB(1 + \lambda)}} - n\left(\frac{m_1}{m_2} + 1\right) - \sqrt{(n + 1)\frac{m_1\left(B^2 + m_3\right)}{B^2(1 - m_3)} + (1 - n)}\right\}\right] \tag{B2}$$

For $n_i \leqq n < 0$,

$$\frac{c_y c_l}{b\alpha} = 2E''(m_1)\left[\sqrt{\left(\frac{4m_1}{AB(1+\lambda)} - \frac{nm_1}{m_2}\right)^2 - n^2} + \frac{m_3 n}{m_1}\cosh^{-1}\left|\frac{4m_1}{nAB(1+\lambda)} - \frac{m_1}{m_2}\right|\right] \tag{B3}$$

For $0 \leqq n \leqq n_j$,

$$\frac{c_y c_l}{b\alpha} = 2E''(m_1)\left\{\sqrt{\left[\frac{4m_1}{AB(1+\lambda)} + \frac{nm_1}{m_2}\right]^2 - n^2} + \frac{m_3 n}{m_1}\cosh^{-1}\left|\frac{4m_1}{nAB(1+\lambda)} + \frac{m_1}{m_2}\right|\right\} \tag{B4}$$

For $n_j \leqq n \leqq 1$,

$$\frac{c_y c_l}{b\alpha} = 2\left(E''(m_1)\left(\sqrt{\left\{\frac{m_1}{B}(1-n)\left[\frac{B^2 - m_3}{B(1+m_3)}\right] + 1\right\}^2 - n^2} + \frac{m_3 n}{m_1}\cosh^{-1}\left|\frac{m_1}{Bn}(1-n)\left[\frac{B^2 - m_3}{B(1+m_3)}\right] + \frac{1}{n}\right|\right) + \frac{4}{\pi m_1\sqrt{\left(m_1 - m_3 + 1 + \frac{m_1 m_3}{B^2}\right)(1+m_3)}}\left\{\frac{m_3}{6\sqrt{1-n}}\left\{\left[\frac{4m_1}{AB(1+\lambda)} + n\left(\frac{m_1}{m_2} + 1\right)\right]^{3/2} - \left[(1-n)\left(\frac{B^2 m_1 - m_1 m_3}{B^2 + B^2 m_3}\right) + 1 + n\right]^{3/2}\right\} + (m_1 - m_3)\sqrt{1-n}\left[\sqrt{\frac{4m_1}{AB(1+\lambda)} + n\left(\frac{m_1}{m_2} + 1\right)} - \sqrt{(1-n)\left(\frac{B^2 m_1 - m_1 m_3}{B^2 + B^2 m_3}\right) + 1 + n}\right]\right\}\right) \tag{B5}$$

where n is the nondimensional spanwise coordinate $\frac{y}{b/2}$, n_i is the value of n at the spanwise station where the tip Mach line from the left half-wing intersects the trailing edge of the left half-wing

$$n_i = \frac{\frac{4}{A(1+\lambda)} - \left[\frac{B}{m_1} + \frac{B^2 + m_3}{B(1 - m_3)}\right]}{\frac{B}{m_2} + \frac{B^2 + m_3}{B(1 - m_3)}}$$

and n_j is the value of n at the spanwise station where the tip Mach line from the right half-wing intersects the trailing edge of the right half-wing

$$n_j = \frac{\left[\frac{B}{m_1} + \frac{B^2 - m_3}{B(1 + m_3)}\right] - \frac{4}{A(1+\lambda)}}{\frac{B}{m_2} + \frac{B^2 - m_3}{B(1 + m_3)}}$$

Rolling moment.- Appropriate integration of the span loading yields the rolling-moment coefficient

$$C_l = -\frac{1}{Sb}\int_{-b/2}^{b/2}\int_{LE}^{TE} C_p y \, dx \, dy = -\frac{1}{Sb}\int_{-b/2}^{b/2} y c_y c_l \, dy \qquad (B6)$$

where the minus sign has been introduced to maintain the usual convention for moments. The following formula results:

$$-c_l = \frac{AB\beta}{3m_1E\left(\sqrt{1-m_1^2}\right)}\left(\frac{m_2^3\omega^3}{2\left(m_2^2-m_1^2\right)^2}\left\{\frac{\left[\left(m_1^2-m_2^2\right)\left(m_1+1\right)+\omega\left(m_2^2-4m_1^2-3m_1^2m_2\right)\right]\sqrt{\left(m_1+1\right)^2\left(m_1^2-m_2^2\right)+2m_2\omega\left(m_1+1\right)\left(m_1^2+m_2\right)+\omega^2m_2^2\left(m_1^2-1\right)}}{\left[\omega m_1\left(m_2+1\right)\right]^2}+\right.\right.$$

$$3m_1-\frac{m_2^2+2m_1^2}{\sqrt{m_2^2-m_1^2}}\left[\sin^{-1}\frac{\left(m_1+1\right)\left(m_1^2-m_2^2\right)+\omega m_2\left(m_1^2+m_2\right)}{m_1m_2\omega\left(m_2+1\right)}-\sin^{-1}\frac{m_1}{\left|m_2\right|}\right]\Bigg\}-$$

$$\frac{1}{3\left(1-m_1\right)^3}\left\{\frac{\left[m_2\left(4m_1^2-1\right)+3m_1^2-\omega m_2\left(m_1-1\right)\right]\sqrt{\left(m_1+1\right)^2\left(m_1^2-m_2^2\right)+2m_2\omega\left(m_1+1\right)\left(m_1^2+m_2\right)+\omega^2m_2^2\left(m_1-1\right)}}{\left[m_1\left(m_2+1\right)\right]^2}-\right.$$

$$\left.\left.\left(1+2m_1^2\right)\sqrt{\frac{1+m_1}{1-m_1}}\left[\frac{\pi}{2}-\sin^{-1}\frac{\left(m_1^2+m_2\right)+\omega m_2\left(m_1-1\right)}{m_1\left(m_2+1\right)}\right]\right\}\right)+\frac{16A\alpha}{\pi\tan\epsilon\sqrt{\left(1+\cot\mu\tan\beta\right)\left[1+\cot\mu\tan\left(\epsilon-\beta\right)\right]}\left(1+\tan\epsilon\tan\beta\right)}\left[\left\{\frac{\tan\epsilon-\tan\beta}{3\left(\cot\delta\tan\epsilon+1\right)}-\right.\right.$$

$$\left.\left.\frac{\tan\epsilon-\tan\beta}{3\left[1-\tan\epsilon\cot\left(\mu+\beta\right)\right]}\right\}\left\{\frac{\frac{2}{A\left(1+\lambda\right)}+\frac{\cot\delta-\cot\epsilon}{2}\frac{2}{A\left(1+\lambda\right)}\left[\tan\epsilon\cot\left(\mu+\beta\right)-1\right]+\frac{\cot\epsilon+\cot\left(\mu+\beta\right)}{2}\left(\cot\delta\tan\epsilon+1\right)}{\cot\delta+\cot\left(\mu+\beta\right)}\right\}^{3/2}-\right.$$

$$\left.\left(\frac{\frac{2}{A\left(1+\lambda\right)}+\frac{\cot\delta-\cot\epsilon}{2}}{\cot\delta+\cot\left(\mu+\beta\right)}\left\{\frac{2\left[\tan\epsilon\cot\left(\mu+\beta\right)-1\right]}{A\left(1+\lambda\right)}+\frac{\cot\epsilon+\cot\left(\mu+\beta\right)}{2}\left(\cot\delta\tan\epsilon+1\right)\right\}\right)^{1/2}\left(\left\{\frac{\tan\beta\left(\cot\delta\tan\epsilon+1\right)}{3}+\right.\right.$$

$$\left.\left.\left[\frac{\tan\beta\left(\cot\delta\tan\epsilon+1\right)}{3}+\tan\epsilon-\tan\beta\right]\left[\frac{1}{4}-\frac{\frac{2\tan\epsilon}{A\left(1+\lambda\right)}}{2\left(\cot\delta\tan\epsilon+1\right)}\right]\right\}\left\{\frac{\cot\epsilon+\cot\left(\mu+\beta\right)}{2}-\frac{2}{A\left(1+\lambda\right)}-\frac{1}{8}+\frac{\frac{\tan\epsilon}{A\left(1+\lambda\right)}}{8\left(\cot\delta\tan\epsilon+1\right)}\right\}+\right.$$

$$\left.\left\{\frac{-\tan\beta\left[1-\tan\epsilon\cot\left(\mu+\beta\right)\right]}{3}+\frac{\tan\epsilon\cot\left(\mu+\beta\right)}{2}\left[\frac{\tan\beta}{3}+\frac{\tan\epsilon-\tan\beta}{1-\tan\epsilon\cot\left(\mu+\beta\right)}\right]\right\}\left\{\frac{\cot\epsilon+\cot\left(\mu+\beta\right)-\frac{2}{A\left(1+\lambda\right)}}{2\left[\cot\delta+\cot\left(\mu+\beta\right)\right]}+\frac{\tan\epsilon\cot\left(\mu+\beta\right)}{4\left[1-\tan\epsilon\cot\left(\mu+\beta\right)\right]}\right\}\right)+$$

(Equation continued on next page)

$$\frac{\left[\frac{\cot\delta\tan\epsilon+1}{2}+\frac{2\tan\epsilon}{A(1+\lambda)}\right]^2}{8\sqrt{\cot\delta\tan\epsilon+1}}\left\{\frac{\tan\beta}{3}+\left(\frac{\tan\beta}{3}+\frac{\tan\epsilon-\tan\beta}{\cot\delta\tan\epsilon+1}\right)\left[\frac{1}{4}-\frac{\frac{\tan\epsilon}{A(1+\lambda)}}{\cot\delta\tan\epsilon+1}\right]\right\}\cos^{-1}\frac{\left[\cot\epsilon+\cot(\mu+\beta)-\frac{4}{A(1+\lambda)}\right](\cot\delta\tan\epsilon+1)}{\cot\delta+\cot(\mu+\beta)}+\frac{2\tan\epsilon}{A(1+\lambda)}-\frac{\cot\delta\tan\epsilon+1}{2}}{\frac{2\tan\epsilon}{A(1+\lambda)}+\frac{\cot\delta\tan\epsilon+1}{2}}-$$

$$\frac{1}{8\sqrt{1-\tan\epsilon\cot(\mu+\beta)}}\left\{\frac{\tan\beta}{3}-\frac{\tan\epsilon\cot(\mu+\beta)}{2\left[1-\tan\epsilon\cot(\mu+\beta)\right]}\left[\frac{\tan\beta}{3}+\frac{\tan\epsilon-\tan\beta}{1-\tan\epsilon\cot(\mu+\beta)}\right]\right\}\cos^{-1}\left\{\frac{\left[\cot\epsilon+\cot(\mu+\beta)-\frac{4}{A(1+\lambda)}\right]\left[1-\tan\epsilon\cot(\mu+\beta)\right]}{\cot\delta+\cot(\mu+\beta)}+\tan\epsilon\cot(\mu+\beta)\right\}+$$

$$\frac{16A\sqrt{1-\tan\epsilon\tan\beta}\tan(\epsilon+\beta)}{\tan\epsilon\sqrt{\left[\cot\mu\tan(\epsilon+\beta)+1\right](1-\cot\mu\tan\beta)}}\left[\frac{\left(\left[\frac{2}{A(1+\lambda)}+\frac{\cot\delta-\cot\epsilon}{2}\right]\left\{\frac{2}{A(1+\lambda)}\left[\tan\epsilon\cot(\mu-\beta)-1\right]+\frac{\cot\epsilon+\cot(\mu-\beta)}{2}(\cot\delta\tan\epsilon+1)\right\}\right)^{3/2}}{-3\left[\cot\delta+\cot(\mu-\beta)\right]^3}\left[\frac{1}{\cot\delta\tan\epsilon+1}+\right.\right.$$

$$\left.\left.\frac{1}{\cot(\mu-\beta)\tan\epsilon-1}\right]-\frac{\left(\left[\frac{2}{A(1+\lambda)}+\frac{\cot\delta-\cot\epsilon}{2}\right]\left\{\frac{2}{A(1+\lambda)}\left[\tan\epsilon\cot(\mu-\beta)-1\right]+\frac{\cot\epsilon+\cot(\mu-\beta)}{2}(\cot\delta\tan\epsilon+1)\right\}\right)^{1/2}}{8\left[\cot\delta+\cot(\mu-\beta)\right]}\times\right.$$

$$\left(\frac{\left[\frac{2\tan\epsilon}{A(1+\lambda)}-\frac{\cot\delta\tan\epsilon+1}{2}\right]\left\{\frac{2\tan\epsilon}{A(1+\lambda)}-\frac{\left[\frac{4}{A(1+\lambda)}-\cot\epsilon+\frac{\cot\delta-\cot(\mu-\beta)}{2}\right](\cot\delta\tan\epsilon+1)}{\cot\delta+\cot(\mu-\beta)}\right\}}{(\cot\delta\tan\epsilon+1)^2}-\right.$$

$$\left.\left.\frac{\cot(\mu-\beta)\tan\epsilon}{\left[\cot(\mu-\beta)\tan\epsilon-1\right]^2}\left\{\cot(\mu-\beta)\tan\epsilon+2\left[\cot(\mu-\beta)\tan\epsilon-1\right]\frac{\frac{2}{A(1+\lambda)}-\frac{\cot\epsilon+\cot(\mu-\beta)}{2}}{\cot\delta+\cot(\mu-\beta)}\right\}\right)+\right.$$

$$\frac{\left[\frac{2\tan\epsilon}{A(1+\lambda)}-\frac{\cot\delta\tan\epsilon+1}{2}\right]\left[\frac{2\tan\epsilon}{A(1+\lambda)}+\frac{\cot\delta\tan\epsilon+1}{2}\right]^2}{16(\cot\delta\tan\epsilon+1)^{5/2}}\cos^{-1}\frac{\frac{2\tan\epsilon}{A(1+\lambda)}-\frac{\frac{4}{A(1+\lambda)}-\cot\epsilon+\frac{\cot\delta-\cot(\mu-\beta)}{2}}{\cot\delta+\cot(\mu-\beta)}(\cot\delta\tan\epsilon+1)}{\frac{2\tan\epsilon}{A(1+\lambda)}+\frac{\cot\delta\tan\epsilon+1}{2}}-$$

$$\left.\frac{\cot(\mu-\beta)\tan\epsilon}{16\left[1-\cot(\mu-\beta)\tan\epsilon\right]^{5/2}}\cos^{-1}\frac{\frac{4}{A(1+\lambda)}\left[\cot(\mu-\beta)\tan\epsilon-1\right]+\cot\epsilon+\cot(\mu-\beta)\tan\epsilon\cot\delta}{\cot\delta+\cot(\mu-\beta)}\right] \tag{57}$$

Stability derivative C_{l_β}.- Differentiation of equation (B7) with respect to β and letting β approach zero yields the stability derivative C_{l_β}:

$$-C_{l_\beta} = \frac{AB}{3m_1^2\left(\sqrt{1-m_1^2}\right)}\left(\frac{m_2^3\omega^3}{2\left(m_2^2-m_1^2\right)^2}\left\{\frac{\left[\left(m_1^2-m_2^2\right)(m_1+1)+\omega\left(m_2^2-4m_1^2-3m_1^2m_2\right)\right]\sqrt{(m_1+1)^2\left(m_1^2-m_2^2\right)+2m_2\omega(m_1+1)\left(m_1^2+m_2\right)+\omega^2m_2^2\left(m_1^2-1\right)}}{\left[\omega m_1(m_2+1)\right]^2}+\right.\right.$$

$$3m_1-\frac{m_2^2+2m_1^2}{\sqrt{m_2^2-m_1^2}}\left[\sin^{-1}\frac{(m_1+1)\left(m_1^2-m_2^2\right)+\omega m_2\left(m_1^2+m_2\right)}{m_1m_2\omega(m_2+1)}-\sin^{-1}\frac{m_1}{|m_2|}\right]\Bigg\}-$$

$$\frac{1}{2(1-m_1)^2}\left\{\frac{\left[m_2\left(4m_1^2-1\right)+3m_1^2-\omega m_2(m_1-1)\right]\sqrt{(m_1+1)^2\left(m_1^2-m_2^2\right)+2m_2\omega(m_1+1)\left(m_1^2+m_2\right)+\omega^2m_2^2\left(m_1^2-1\right)}}{\left[m_1(m_2+1)\right]^2}-\right.$$

$$\left.\left.\left(1+2m_1^2\right)\sqrt{\frac{1+m_1}{1-m_1}}\left[\frac{\pi}{2}-\sin^{-1}\frac{\left(m_1^2+m_2\right)+\omega m_2(m_1-1)}{m_1(m_2+1)}\right]\right\}\right)-$$

$$\frac{8A\omega}{\pi}\frac{\cos^2\mu}{(1+\tan\epsilon\cot\mu)^{3/2}}\left(\left[\frac{\cot\delta-\cot\epsilon}{2}+\frac{2}{A(1+\lambda)}\right.\right.\frac{2(\tan\epsilon\cot\mu-1)}{A(1+\lambda)}+\left.\left.\frac{(\cot\epsilon+\cot\mu)(\cot\delta\tan\epsilon+1)}{2}\right]^{-3/2}\left[\frac{\tan\epsilon}{3(\cot\delta\tan\epsilon+1)}-\frac{\tan\epsilon}{3(1-\cot\mu\tan\epsilon)}\right]-\right.$$

$$\left.\frac{\left\{\left[\frac{\cot\delta-\cot\epsilon}{2}+\frac{2}{A(1+\lambda)}\right]\left[\frac{2(\tan\epsilon\cot\mu-1)}{A(1+\lambda)}+\frac{1}{2}(\cot\epsilon+\cot\mu)(\cot\delta\tan\epsilon+1)\right]\right\}^{1/2}}{\cot\delta+\cot\mu}\left\{\tan\epsilon\left[\frac{1}{\lambda}-\frac{\tan\epsilon}{A(1+\lambda)(\cot\delta\tan\epsilon+1)}\right]\left[\frac{\cot\epsilon+\cot\mu}{2}-\frac{2}{A(1+\lambda)}\right]-\frac{1}{8}+\right.\right.$$

(Equation continued on next page)

$$\frac{\tan\epsilon}{2A(1+\lambda)(\cot\delta\tan\epsilon+1)}\Bigg]+\frac{\tan\epsilon}{1-\cot\mu\tan\epsilon}\,\frac{\cot\mu\tan\epsilon}{2}\left[\frac{\cot\epsilon+\cot\mu}{2}-\frac{2}{A(1+\lambda)}+\frac{\cot\mu\tan\epsilon}{4(1-\cot\mu\tan\epsilon)}\right]\Bigg\}+$$

$$\left\{\left[\frac{\cot\delta\tan\epsilon+1}{2}+\frac{2\tan\epsilon}{A(1+\lambda)}\right]^2\frac{\tan\epsilon}{8\sqrt{\cot\delta\tan\epsilon+1}}\left[\frac{1}{4}-\frac{\tan\epsilon}{A(1+\lambda)(\cot\delta\tan\epsilon+1)}\right]\right\}\cos^{-1}\frac{\left[\cot\epsilon+\cot\mu-\frac{4}{A(1+\lambda)}\right]\left[\cot\delta\tan\epsilon+1\right]}{\cot\delta+\cot\mu}+\frac{2\tan\epsilon}{A(1+\lambda)}-\frac{\cot\delta\tan\epsilon+1}{2}}{\frac{2\tan\epsilon}{A(1+\lambda)}+\frac{\cot\delta\tan\epsilon+1}{2}}-$$

$$\frac{1}{8\sqrt{1-\cot\mu\tan\epsilon}}\left(-\frac{\cot\mu\tan\epsilon}{2(1-\cot\mu\tan\epsilon)}\,\frac{\tan\epsilon}{1-\cot\mu\tan\epsilon}\right)\cos^{-1}\left[\frac{\cot\epsilon+\cot\mu-\frac{4}{A(1+\lambda)}}{\cot\delta+\cot\mu}(1-\cot\mu\tan\epsilon)+\cot\mu\tan\epsilon\right]\Bigg)+$$

$$\frac{16m}{\pi\tan\epsilon(1+\tan\epsilon\cot\mu)^{1/2}}\left[\frac{\frac{\cot\delta-\cot\epsilon}{2}+\frac{2}{A(1+\lambda)}\,\frac{2}{A(1+\lambda)}(\tan\epsilon\cot\mu-1)+\frac{\cot\epsilon+\cot\mu}{2}(\cot\delta\tan\epsilon+1)}{\cot\delta+\cot\mu}\right]^{3/2}\left[\frac{-1}{3(\cot\delta\tan\epsilon+1)}+\frac{1}{3(1-\cot\mu\tan\epsilon)}+\frac{\csc^2\mu\tan^2\epsilon}{3(1-\cot\mu\tan\epsilon)^2}\right]+$$

$$\left(\frac{\tan\epsilon}{\cot\delta\tan\epsilon+1}-\frac{\tan\epsilon}{1-\cot\mu\tan\epsilon}\right)\csc^2\mu\left[\frac{\frac{\cot\delta-\cot\epsilon}{2}+\frac{2}{A(1+\lambda)}\,\frac{2(\tan\epsilon\cot\mu-1)}{A(1+\lambda)}+\frac{\cot\epsilon+\cot\mu}{2}(\cot\delta\tan\epsilon+1)}{\cot\delta+\cot\mu}\right]^{1/2}\frac{\frac{\cot\delta-\cot\epsilon}{2}+\frac{2}{A(1+\lambda)}}{\cot\delta+\cot\mu}\left\{-\frac{\left[\frac{2\tan\epsilon}{A(1+\lambda)}+\frac{\cot\delta\tan\epsilon+1}{2}\right]}{2(\cot\delta+\cot\mu)}+\right.$$

$$\left.\frac{2(\tan\epsilon\cot\mu-1)}{A(1+\lambda)}+\frac{(\cot\epsilon+\cot\mu)(\tan\epsilon\cot\delta+1)}{2}\right\}+\left[\frac{\cot\delta-\cot\epsilon}{2}+\frac{2}{A(1+\lambda)}\right]^{1/2}\csc^2\mu\left\{\frac{\frac{2\tan\epsilon}{A(1+\lambda)}+\frac{\cot\delta\tan\epsilon+1}{2}}{2\left[\frac{2(\tan\epsilon\cot\mu-1)}{A(1+\lambda)}+\frac{(\cot\epsilon+\cot\mu)(\cot\delta\tan\epsilon+1)}{2}\right]^{1/2}(\cot\delta+\cot\mu)}-\right.$$

$$\left.\frac{\left[\frac{2(\tan\epsilon\cot\mu-1)}{A(1+\lambda)}+\frac{(\cot\epsilon+\cot\mu)(\cot\delta\tan\epsilon+1)}{2}\right]^{1/2}}{(\cot\delta+\cot\mu)^2}\right\}\left\{\tan\epsilon\left[\frac{1}{4}-\frac{\tan\epsilon}{A(1+\lambda)(\cot\delta\tan\epsilon+1)}\right]\left[\frac{\cot\epsilon+\cot\mu}{2}-\frac{2}{A(1+\lambda)}\right]-\frac{1}{8}+\frac{\tan\epsilon}{2A(1+\lambda)(\cot\delta\tan\epsilon+1)}\right]+$$

(Equation continued on next page)

$$\frac{\tan^2\epsilon\cot\mu}{2(1-\cot\mu\tan\epsilon)}\left[\frac{\cot\epsilon+\cot\mu}{2}-\frac{2}{A(1+\lambda)}\right]\left[\frac{\cot\epsilon+\cot\mu}{2(\cot\delta+\cot\mu)}+\frac{\cot\mu\tan\epsilon}{4(1-\cot\mu\tan\epsilon)}\right]-\frac{\left\{\left[\frac{\cot\delta-\cot\epsilon}{2}+\frac{2}{A(1+\lambda)}\right]\left[\frac{2}{A(1+\lambda)}(\tan\epsilon\cot\mu-1)+\frac{\cot\epsilon+\cot\mu}{2}(\cot\delta\tan\epsilon+1)\right]\right\}^{1/2}}{\cot\delta+\cot\mu}\left(\left\{\frac{\cot\delta\tan\epsilon+1}{3}+\left(\frac{\cot\delta\tan\epsilon+1}{3}-1\right)\left[\frac{1}{4}-\frac{\tan\epsilon}{A(1+\lambda)(\cot\delta\tan\epsilon+1)}\right]\right\}\left[\frac{\cot\epsilon+\cot\mu}{2(\cot\delta+\cot\mu)}-\frac{1}{8}+\frac{\tan\epsilon}{2A(1+\lambda)(\cot\delta\tan\epsilon+1)}\right]+\tan\epsilon\left[\frac{1}{4}-\frac{\tan\epsilon}{A(1+\lambda)(\cot\delta\tan\epsilon+1)}\right]\frac{\csc^2\mu\left[\frac{\cot\epsilon-\cot\delta}{2}-\frac{2}{A(1+\lambda)}\right]}{2(\cot\delta+\cot\mu)^2}+\left\{\frac{\cot\mu\tan\epsilon-1}{3}+\frac{\cot\mu\tan\epsilon}{8}\left[\frac{1}{3}-\frac{1}{1-\cot\mu\tan\epsilon}-\frac{\csc^2\mu\tan^2\epsilon}{(1-\cot\mu\tan\epsilon)^2}\right]-\frac{\tan^2\epsilon\csc^2\mu}{2(1-\cot\mu\tan\epsilon)}\right\}\left[\frac{\cot\epsilon+\cot\mu}{2}-\frac{2}{A(1+\lambda)}\right]\left[\frac{\cot\mu\tan\epsilon}{4(1-\cot\mu\tan\epsilon)}\right]+\frac{\tan^2\epsilon\csc^2\mu\cot\mu}{2(1-\cot\mu\tan\epsilon)}\left[\frac{\cot\epsilon-\cot\delta}{2}-\frac{2}{A(1+\lambda)}\right]\left[\frac{\cot\epsilon-\cot\delta}{2(\cot\delta+\cot\mu)^2}-\frac{\tan\epsilon}{4(1-\cot\mu\tan\epsilon)^2}\right]\right)+\frac{\left[\frac{\cot\delta\tan\epsilon+1}{2}+\frac{2\tan\epsilon}{A(1+\lambda)}\right]^2}{8\sqrt{\cot\delta\tan\epsilon+1}}\left\{\frac{1}{3}+\left(\frac{1}{3}-\frac{1}{\cot\delta\tan\epsilon+1}\right)\left[\frac{1}{4}-\frac{\tan\epsilon}{A(1+\lambda)(\cot\delta\tan\epsilon+1)}\right]\right\}\cos^{-1}\left\{\left[\cot\epsilon+\cot\mu-\frac{4}{A(1+\lambda)}\right](\cot\delta\tan\epsilon+1)\frac{\frac{2\tan\epsilon}{A(1+\lambda)}-\frac{\cot\delta\tan\epsilon+1}{2}}{(\cot\delta+\cot\mu)\left[\frac{2\tan\epsilon}{A(1+\lambda)}+\frac{\cot\delta\tan\epsilon+1}{2}\right]}+\frac{\left[\frac{\cot\delta\tan\epsilon+1}{2}+\frac{2\tan\epsilon}{A(1+\lambda)}\right]^2}{8\sqrt{\cot\delta\tan\epsilon+1}}\left\{\frac{\tan\epsilon\csc^2\mu}{\cot\delta\tan\epsilon+1}\left[\frac{1}{4}-\frac{\tan\epsilon}{A(1+\lambda)(\cot\delta\tan\epsilon+1)}\right]\right\}\left\{\frac{\left[\cot\delta-\cot\epsilon+\frac{4}{A(1+\lambda)}\right]\sqrt{\cot\delta\tan\epsilon+1}}{(\cot\delta+\cot\mu)\sqrt{\frac{8(\cot\epsilon+\tan\epsilon\cot\delta\cot\mu)}{A(1+\lambda)}}-(\cot\epsilon+\cot\mu)(\sec\epsilon-\sec^2\delta\tan\epsilon)+\frac{16}{A^2(1+\lambda)^2}(\tan\epsilon\cot\mu-1)}\right\}-\left(\frac{\cot\mu\tan^3\epsilon\csc^2\mu}{32(1-\cot\mu\tan\epsilon)^{7/2}}+\frac{1}{8(1-\cot\mu\tan\epsilon)^{1/2}}\left\{\frac{1}{3}+\frac{\tan^2\epsilon\csc^2\mu}{(1-\cot\mu\tan\epsilon)^2}\left[\frac{1}{2}+\frac{\tan\epsilon\cot\mu}{2(1-\cot\mu\tan\epsilon)}\right]-\frac{\cot\mu\tan\epsilon}{2(1-\cot\mu\tan\epsilon)}\left[\frac{1}{3}-\frac{1}{1-\cot\mu\tan\epsilon}-\frac{\csc^2\mu\tan^2\epsilon}{(1-\cot\mu\tan\epsilon)^2}\right]\right\}\right)\cos^{-1}\left[\frac{\cot\epsilon+\cot\mu-\frac{4}{A(1+\lambda)}}{\cot\delta+\cot\mu}(1-\cot\mu\tan\epsilon)+\cot\mu\tan\epsilon\right]-\frac{\cot\mu\tan^2\epsilon}{16(1-\cot\mu\tan\epsilon)^{3/2}}\left(\frac{\csc^2\mu\left[\cot\epsilon-\cot\delta-\frac{4}{A(1+\lambda)}\right]\cot\delta\tan\epsilon+1}{\cot\delta+\cot\mu}\right)\Bigg]+$$

(Equation continued on next page)

$$\frac{16A\alpha}{\pi\tan\epsilon}\left[\frac{1}{\sqrt{\cot\mu\tan\epsilon+1}}+\frac{\tan^2\epsilon\sec^2\mu}{2(\cot\mu\tan\epsilon+1)^{3/2}}\right]\left[\frac{\left\{\left[\frac{2}{A(1+\lambda)}+\frac{\cot\delta-\cot\epsilon}{2}\right]\left[\frac{2}{A(1+\lambda)}(\cot\mu\tan\epsilon-1)+\left(\frac{\cot\epsilon+\cot\mu}{2}\right)(\cot\delta\tan\epsilon+1)\right]\right\}^{3/2}}{-3(\cot\delta+\cot\mu)^3}\left(\frac{1}{\cot\delta\tan\epsilon+1}+\frac{1}{\cot\mu\tan\epsilon-1}\right)-\right.$$

$$\frac{\left\{\left[\frac{2}{A(1+\lambda)}+\frac{\cot\delta-\cot\epsilon}{2}\right]\left[\frac{2}{A(1+\lambda)}(\cot\mu\tan\epsilon-1)+\frac{\cot\epsilon+\cot\mu}{2}(\cot\delta\tan\epsilon+1)\right]\right\}^{1/2}}{8(\cot\delta+\cot\mu)}\left(\frac{\left[\frac{2\tan\epsilon}{A(1+\lambda)}-\frac{\cot\delta\tan\epsilon+1}{2}\right]\left\{\frac{2\tan\epsilon}{A(1+\lambda)}-\frac{\left[\frac{4}{A(1+\lambda)}-\cot\epsilon+\frac{\cot\delta-\cot\mu}{2}\right](\cot\delta\tan\epsilon+1)}{\cot\delta+\cot\mu}\right\}}{(\cot\delta\tan\epsilon+1)^2}-\right.$$

$$\left.\left.\frac{\cot\mu\tan\epsilon}{(\cot\delta\tan\epsilon-1)^2}\left[\cot\mu\tan\epsilon+2(\cot\mu\tan\epsilon-1)\frac{\frac{2}{A(1+\lambda)}-\frac{\cot\epsilon+\cot\mu}{2}}{\cot\delta+\cot\mu}\right]\right)+\frac{\left[\frac{2\tan\epsilon}{A(1+\lambda)}-\frac{\cot\delta\tan\epsilon+1}{2}\right]\left[\frac{2\tan\epsilon}{A(1+\lambda)}+\frac{\cot\delta\tan\epsilon+1}{2}\right]^2}{16(\cot\delta\tan\epsilon+1)^{5/2}}\right.$$

$$\cos^{-1}\frac{\frac{2\tan\epsilon}{A(1+\lambda)}-\frac{\frac{4}{A(1+\lambda)}-\cot\epsilon+\frac{\cot\delta-\cot\mu}{2}}{\cot\delta+\cot\mu}(\cot\delta\tan\epsilon+1)}{\frac{2\tan\epsilon}{A(1+\lambda)}+\frac{\cot\delta\tan\epsilon+1}{2}}-\frac{\cot\mu\tan\epsilon}{16(1-\cot\mu\tan\epsilon)^{5/2}}\cos^{-1}\frac{\frac{4}{A(1+\lambda)}(\cot\mu\tan\epsilon-1)+\cot\epsilon+\cot\mu\tan\epsilon\cot\delta}{\cot\delta+\cot\mu}\Bigg]+$$

$$\frac{16A\alpha}{\pi(\cot\mu\tan\epsilon+1)^{1/2}}\left[\frac{\left[\frac{2}{A(1+\lambda)}+\frac{\cot\delta-\cot\epsilon}{2}\right]^{3/2}\left[\frac{2}{A(1+\lambda)}(\cot\pi\tan\epsilon-1)+\frac{\cot\epsilon+\cot\mu}{2}(\cot\delta\tan\epsilon+1)\right]^{1/2}}{-2(\cot\delta+\cot\pi)^3}\left[\frac{2(\tan\epsilon\sec^2\mu)}{A(1+\lambda)}+\frac{\sec^2\mu(\cot\delta\tan\epsilon+1)}{2}\right]\left(\frac{1}{\cot\delta\tan\epsilon+1}+\right.\right.$$

$$\frac{1}{\cot\mu\tan\epsilon-1}\Bigg)+\sec^2\mu\frac{\left\{\left[\frac{2}{A(1+\lambda)}+\frac{\cot\delta-\cot\epsilon}{2}\right]\left[\frac{2}{A(1+\lambda)}(\cot\pi\tan\epsilon-1)+\frac{\cot\epsilon+\cot\mu}{2}(\cot\delta\tan\epsilon+1)\right]\right\}^{3/2}}{(\cot\delta+\cot\mu)^3}\left[\frac{1}{\cot\delta+\cot\mu}\left(\frac{1}{\cot\delta\tan\epsilon+1}+\right.\right.$$

$$\left.\left.\left.\frac{1}{\cot\mu\tan\epsilon-1}\right)+\frac{\tan\epsilon}{3(\cot\mu\tan\epsilon-1)^2}\right]-\left(\frac{\left[\frac{2}{A(1+\lambda)}+\frac{\cot\delta-\cot\epsilon}{2}\right]^{1/2}\left[\frac{2\tan\epsilon}{A(1+\lambda)}+\frac{\cot\delta\tan\epsilon+1}{2}\right]}{16(\cot\delta+\cot\mu)\left[\frac{2}{A(1+\lambda)}(\cot\pi\tan\epsilon-1)+(\cot\epsilon+\cot\mu)\frac{\cot\delta\tan\epsilon+1}{2}\right]^{1/2}}\right.\right.$$

(Equation continued on next page)

$$\frac{\left\{\left[\frac{2}{A(1+\lambda)}+\frac{\cot\delta-\cot\epsilon}{2}\right]\left[\frac{2}{A(1+\lambda)}(\cot\mu\tan\epsilon-1)+(\cot\epsilon+\cot\mu)\frac{\cot\delta\tan\epsilon+1}{2}\right]\right\}^{1/2}}{\delta(\cot\delta+\cot\mu)^2}\Bigg)$$

$$\cos^2\mu\left(\frac{\left[\frac{2\tan\epsilon}{A(1+\lambda)}-\frac{\cot\delta\tan\epsilon+1}{2}\right]\left[\frac{2\tan\epsilon}{A(1+\lambda)}-\frac{\left[\frac{4}{A(1+\lambda)}-\cot\epsilon+\frac{\cot\delta-\cot\mu}{2}\right](\cot\delta\tan\epsilon+1)}{\cot\delta+\cot\mu}\right]}{(\cot\delta\tan\epsilon+1)^2}-\frac{\cot\mu\tan\epsilon}{(\cot\mu\tan\epsilon-1)^2}\left[\frac{2}{\delta(\cot\mu\tan\epsilon-1)}\frac{\frac{2}{A(1+\lambda)}-\frac{\cot\epsilon+\cot\mu}{2}}{\cot\delta+\cot\mu}+\cot\mu\tan\epsilon\right]\right)-$$

$$\frac{\left\{\left[\frac{2}{A(1+\lambda)}+\frac{\cot\delta-\cot\epsilon}{2}\right]\left[\frac{2}{A(1+\lambda)}(\cot\mu\tan\epsilon-1)+(\cot\epsilon+\cot\mu)\frac{\cot\delta\tan\epsilon+1}{2}\right]\right\}^{1/2}}{\delta(\cot\delta+\cot\mu)}\cos^2\mu\left\{\frac{\left[\frac{2\tan\epsilon}{A(1+\lambda)}-\frac{\cot\delta\tan\epsilon+1}{2}\right]\left[\cot\delta-\cot\epsilon+\frac{4}{A(1+\lambda)}\right]}{(\cot\delta+\cot\mu)^2(\cot\delta\tan\epsilon+1)}-\left[\frac{\tan\epsilon}{(\cot\mu\tan\epsilon-1)^2}-\right.\right.$$

$$\left.\frac{2\tan^2\epsilon\cot\mu}{(\cot\mu\tan\epsilon-1)^3}\right]\left[\cot\mu\tan\epsilon+2(\cot\mu\tan\epsilon-1)\frac{\frac{2}{A(1+\lambda)}-\frac{\cot\epsilon+\cot\mu}{2}}{\cot\delta+\cot\mu}\right]-\frac{\cot\mu\tan\epsilon}{(\cot\mu\tan\epsilon-1)^2}\left[\tan\epsilon+2\tan\epsilon\frac{\frac{2}{A(1+\lambda)}-\frac{\cot\epsilon+\cot\mu}{2}}{\cot\delta+\cot\mu}-2(\cot\mu\tan\epsilon-1)\frac{\frac{\cot\delta-\cot\epsilon}{2}+\frac{2}{A(1+\lambda)}}{(\cot\delta+\cot\mu)^2}\right]\Bigg\}-$$

$$\frac{\left[\frac{2\tan\epsilon}{A(1+\lambda)}-\frac{\cot\delta\tan\epsilon+1}{2}\right]\left[\frac{2\tan\epsilon}{A(1+\lambda)}+\frac{\cot\delta\tan\epsilon+1}{2}\right]^2}{16(\cot\delta\tan\epsilon+1)^{5/2}}\frac{\sec^2\mu(\cot\delta\tan\epsilon+1)\frac{\cot\delta-\cot\epsilon+\frac{4}{A(1+\lambda)}}{(\cot\delta+\cot\mu)^2}}{\sqrt{\left[\frac{2\tan\epsilon}{A(1+\lambda)}+\frac{\cot\delta\tan\epsilon+1}{2}\right]^2-\left[\frac{2\tan\epsilon}{A(1+\lambda)}-\frac{\frac{4}{A(1+\lambda)}-\cot\epsilon+\frac{\cot\delta-\cot\mu}{2}}{\cot\delta+\cot\mu}(\cot\delta\tan\epsilon+1)\right]^2}}-$$

$$\frac{\sec^2\mu\tan\epsilon}{16(1-\cot\mu\tan\epsilon)^{3/2}}\left(1+\frac{8}{5}\frac{\tan\epsilon\cot\mu}{1-\cot\mu\tan\epsilon}\right)\cos^{-1}\frac{\frac{4}{A(1+\lambda)}(\cot\mu\tan\epsilon-1)+\cot\epsilon+\cot\mu\tan\epsilon\cot\delta}{\cot\delta+\cot\mu}+$$

$$\left.\frac{\cot\mu\tan\epsilon\sec^2\mu}{16(1-\cot\mu\tan\epsilon)^{5/2}}\frac{\frac{4(1+\cot\delta\tan\epsilon)}{A(1+\lambda)}+\tan\epsilon(\cot^2\delta-\cot^2\epsilon)}{(\cot\delta+\cot\mu)\sqrt{(\cot\delta+\cot\mu)^2-\left[\frac{4}{A(1+\lambda)}(\cot\mu\tan\epsilon-1)+\cot\epsilon+\cot\mu\tan\epsilon\cot\delta\right]^2}}\right] \tag{B8}$$

Equations (B7) and (B8) could be simplified somewhat but the effort involved and the resultant saving of calculation time did not appear to justify such action.

APPENDIX C

DERIVATION OF EQUATIONS FOR THE PRESSURE DISTRIBUTION FOR WINGS WITH ONE LEADING EDGE SUBSONIC AND ONE LEADING EDGE SUPERSONIC

Equations for the pressure distributions for wings with one leading edge subsonic and one leading edge supersonic are derived. The plan form under consideration is shown in figure 7.

The expression for the perturbation potential at any point (u_w, v_w) on the wing is given by equation (A8) of appendix A.

$$\phi(u_w,v_w) = \frac{V\alpha}{\pi M}\iint_{S_W} \frac{du\,dv}{\sqrt{(u_w - u)(v_w - v)}}$$

It has been shown in reference 26 (see pages 29 and 30) that the perturbation velocity $\partial\phi/\partial s$ may be expressed as

$$\frac{\partial\phi}{\partial s} = \frac{V\alpha}{2B\pi}\int_{P_1(u,v)}^{P_2(u,v)} \frac{dv - du}{\sqrt{(u_w - u)(v_w - v)}} + f(u_w,v_w) \qquad (C1)$$

where the integral in equation (C1) is a line integral evaluated along a segment of the wing leading edge or edges and $f(u_w,v_w)$ is a function that can assume different values depending on the boundary conditions imposed on the flow. The values that $f(u_w,v_w)$ assumes for the purposes of the present paper are as follows:

(a) For wing regions not influenced by a wing tip or by a subsonic leading edge and for wing regions influenced by a wing tip where the Kutta-Joukowski condition is satisfied,

$$f(u_w,v_w) = 0 \qquad (C2)$$

(b) For wing regions influenced by the wing tip on the right half-wing but not influenced by a subsonic leading edge on the left half-wing,

$$f(u_w,v_w) = \frac{V\alpha}{B\pi}\left(1 - k_3\right)\sqrt{\frac{v_w + \frac{k_3(v_w - d)}{k_1}}{u_w - k_3(v_w - d)}} \tag{C3}$$

(c) For wing regions influenced by a subsonic leading edge on the left half-wing but not influenced by the wing tip on the right half-wing,

$$f(u_w,v_w) = \frac{V\alpha}{B\pi}\left(1 - \frac{1}{k_2}\right)\sqrt{\frac{u_w + \frac{k_1 u_w}{k_2}}{v_w - \frac{u_w}{k_2}}} \tag{C4}$$

(d) For wing regions influenced by both a subsonic leading edge on the left half-wing and the wing tip on the right half-wing,

$$f(u_w,v_w) = \frac{V\alpha}{B\pi}\left[\left(1 - k_3\right)\sqrt{\frac{v_w + \frac{k_3(v_w - d)}{k_1}}{u_w - k_3(v_w - d)}} + \left(1 - \frac{1}{k_2}\right)\sqrt{\frac{u_w + \frac{k_1 u_w}{k_2}}{v_w - \frac{u_w}{k_2}}}\right] \tag{C5}$$

(The terms right half-wing and left half-wing refer to those portions of the wing plan form that are in the (x,y) quadrant and in the (x, - y) quadrant, respectively. (See fig. 1.))

The pressure coefficient is related to the velocity $\partial\phi/\partial s$ as follows:

$$C_P = \frac{4}{V}\frac{\partial\phi}{\partial s}$$

or by using equation (C1)

$$C_P = 4\left[\frac{\alpha}{2B\pi}\int_{P_1(u,v)}^{P_2(u,v)} \frac{dv - du}{\sqrt{(v_w - v)(u_w - u)}} + \frac{1}{V} f(u_w,v_w)\right] \tag{C6}$$

Equation (C6) gives the pressure coefficient in the u_w,v_w coordinate system which is related to the x,y body-axes system of the present report by equations (A15) of appendix A. Inasmuch as it is more convenient to use the body-axes system in determining loadings and moments, the final expressions for C_p are given in the x,y notation.

The expressions for the pressure coefficients for regions IV to VIII (see fig. 7) may now be derived by using equations (C6), (A15) and the appropriate value of the function $f(u_w,v_w)$ as given by equations (C2), (C3), (C4), and (C5).

Region IV.- Region IV is the hatched portion of the wing shown below.

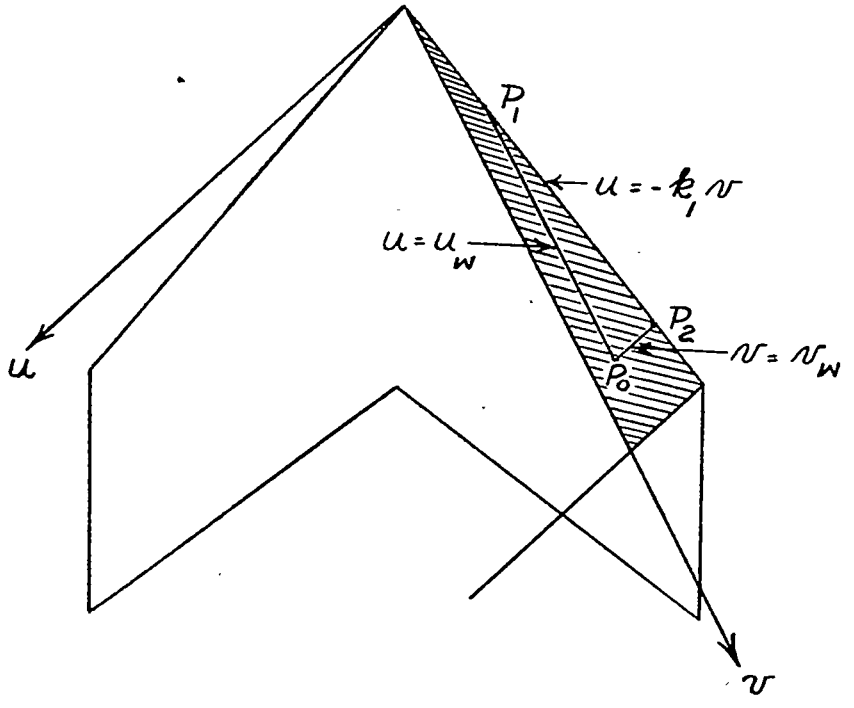

Point	u coordinate	v coordinate
P_0	u_w	v_w
P_1	u_w	$-u_w/k_1$
P_2	$-k_1 v_w$	v_w

Inasmuch as region IV is not influenced by either wing tip or by the subsonic leading edge on the left half-wing, the appropriate value of $f(u_w, v_w)$ is given by equation (C2). When the procedure given in reference 26 is followed and the appropriate relations and limits are substituted into equation (C6), the expression for the pressure coefficient in region IV may be written as follows:

$$(C_p)_{IV} = \frac{2\alpha}{B\pi} \int_{-u_w/k_1}^{v_w} \frac{(1 + k_1)dv}{\sqrt{(v_w - v)(u_w + k_1 v)}} \tag{C7}$$

Performance of the integration indicated in equation (C7) yields

$$(C_p)_{IV} = \frac{2\alpha}{B} \frac{k_1 + 1}{\sqrt{k_1}} \tag{C8}$$

Region V.- Region V is the hatched portion of the wing shown below.

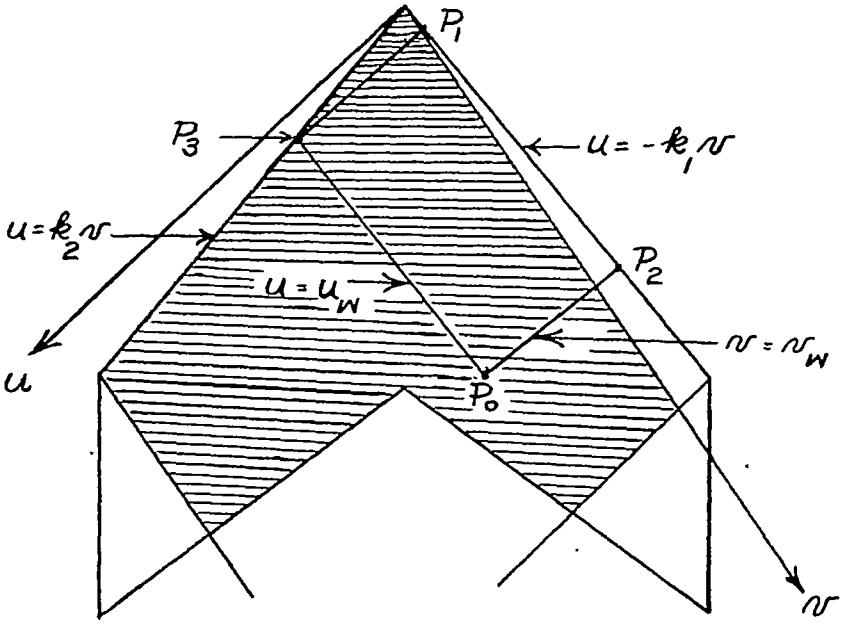

Point	u coordinate	v coordinate
P_0	u_w	v_w
P_1	$-k_1 u_w/k_2$	u_w/k_2
P_2	$-k_1 v_w$	v_w
P_3	u_w	u_w/k_2

Inasmuch as region V is influenced by a subsonic leading edge on the left half-wing, equation (C4) gives the appropriate value of $f(u_w, v_w)$. Upon substitution of the proper functional relations and limits into equation (C6) the pressure coefficient is given as

$$(C_p)_V = \frac{4\alpha}{B\pi}\left\{\frac{1}{2}\int_{u_w/k_2}^{v_w} \frac{(k_1 + 1)\,dv}{\sqrt{(u_w + k_1 v)(v_w - v)}} + \left(1 - \frac{1}{k_2}\right)\sqrt{\frac{u_w + \dfrac{k_1 u_w}{k_2}}{v_w - \dfrac{u_w}{k_2}}}\right\} \tag{C9}$$

Performing the integration indicated in equation (C9) and application of equations (A15) yields

$$(C_p)_V = \frac{2\alpha}{B\pi}\frac{k_1 + 1}{\sqrt{k_1}}\cos^{-1}\frac{\left[\left(1 + \frac{2k_1}{k_2}\right)(1 - B\tan\beta) - k_1(1 + B\tan\beta)\right]x - \left[\left(1 + \frac{2k_1}{k_2}\right)(B + \tan\beta) + k_1(B - \tan\beta)\right]y}{\left[(1 - B\tan\beta) + k_1(1 + B\tan\beta)\right]x + \left[k_1(B - \tan\beta) - (B + \tan\beta)\right]y} +$$

$$\frac{4\alpha}{B\pi}\frac{k_2 - 1}{k_2}\sqrt{\frac{\left(1 + \frac{k_1}{k_2}\right)(1 - B\tan\beta)x - \left(1 + \frac{k_1}{k_2}\right)(B + \tan\beta)y}{\left[(1 + B\tan\beta) - \frac{1}{k_2}(1 - B\tan\beta)\right]x + \left[(B - \tan\beta) + \frac{1}{k_2}(B + \tan\beta)\right]y}} \tag{C10}$$

Region VI.- Region VI is the hatched portion of the wing shown below.

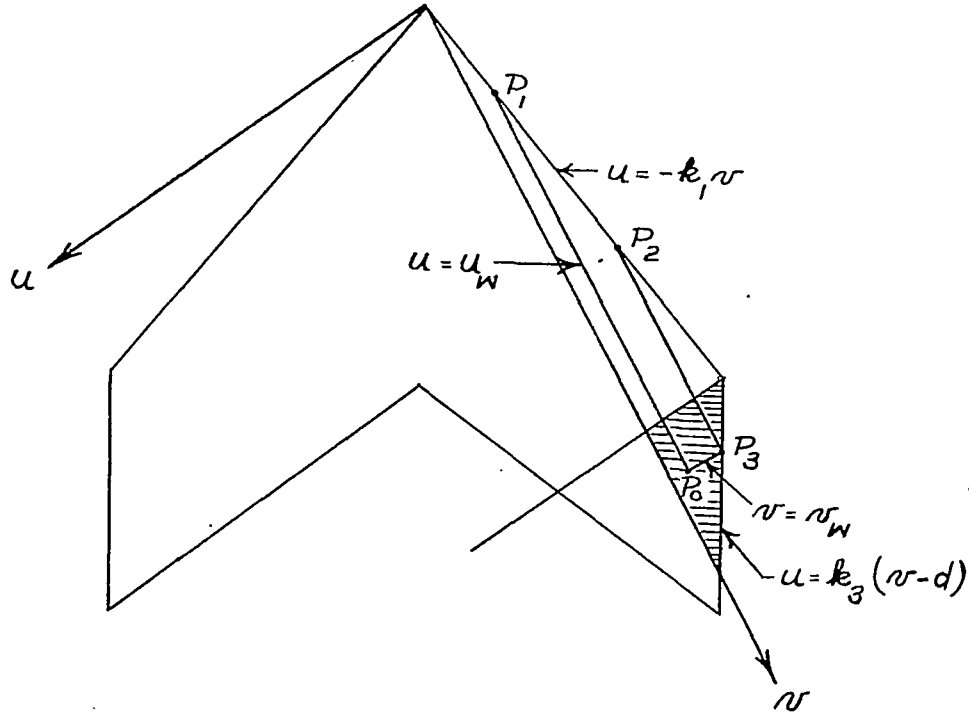

Point	u coordinate	v coordinate
P_0	u_w	v_w
P_1	u_w	$-u_w/k_1$
P_2	$k_3(v_w - d)$	$\frac{k_3(v - d)}{-k_1}$
P_3	$k_3(v_w - d)$	v_w

Region VI is influenced by the wing tip on the right half-wing; therefore, the appropriate form of $f(u_w, v_w)$ is given by equation (C3). Upon substitution of limits and relations into equation (C6), the pressure coefficient in region VI is given by

$$(C_p)_{VI} = \frac{4\alpha}{B\pi}\left\{\frac{1}{2}\int_{\frac{-u_w}{k_1}}^{\frac{-k_3(v_w-d)}{k_1}} \frac{(k_1+1)dv}{\sqrt{(u_w+k_1v)(v_w-v)}} + (1-k_3)\sqrt{\frac{v_w+k_3\left(\frac{v_w-d}{k_1}\right)}{u_w-k_3(v_w-d)}}\right\} \tag{C11}$$

Performing the integration indicated in equation (C11) and application of equations (A15) yields

$$(C_p)_{VI} = \frac{2\alpha}{B}\frac{k_1+1}{\sqrt{k_1}}\left\{1-\frac{2}{\pi}\tan^{-1}\sqrt{\frac{(k_1+k_3)(1+B\tan\beta)x+(k_1+k_3)(B-\tan\beta)y-\frac{Bb}{\cos^2\beta(1+B\tan\beta)}}{\frac{2B}{\cos^2\beta(1+B\tan\beta)}\left(\frac{b}{2}-y\right)}}\right\}+$$

$$\frac{4\alpha}{B\pi}(1-k_3)\sqrt{\frac{\left(1+\frac{k_3}{k_1}\right)(1+B\tan\beta)x+\left(1+\frac{k_3}{k_1}\right)(B-\tan\beta)y-\frac{Bb}{k_1\cos^2\beta(1+B\tan\beta)}}{\frac{2B}{\cos^2\beta(1+B\tan\beta)}\left(\frac{b}{2}-y\right)}} \tag{C12}$$

Region VII.- P ı VII is the hatched portion of the wing shown below.

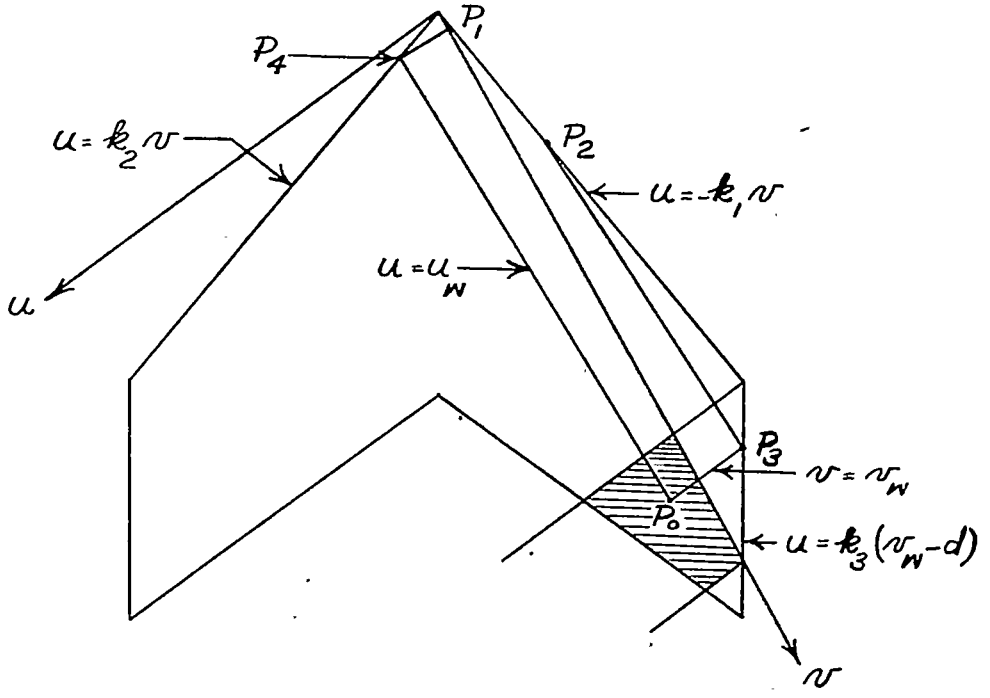

Point	u coordinate	v coordinate
P_0	u_w	v_w
P_1	$-k_1u_w/k_2$	u_w/k_2
P_2	$k_3(v_w - d)$	$\frac{k_3(v_w - d)}{-k_1}$
P_3	$k_3(v_w - d)$	v_w
P_4	u_w	u_w/k_2

Region VII is influenced by both the wing tip on the right half-wing and by the subsonic leading edge on the left half-wing; equation (C5) gives the proper value of $f(u_w, v_w)$. Substitution of limits and functional relations into equation (C6) yields

$$(C_p)_{VII} = 4\alpha\left\{\frac{1}{2B\pi}\int_{\frac{u_w}{k_2}}^{\frac{-k_3(v_w-d)}{k_1}} \frac{(k_1+1)\,dv}{\sqrt{(u_w+k_1v)(v_w-v)}} + \frac{1}{B\pi}\left[(1-k_3)\sqrt{\frac{v_w+\frac{k_3(v_w-d)}{k_1}}{u_w-k_3(v_w-d)}} + \frac{k_2-1}{k_2}\sqrt{\frac{u_w+\frac{k_1u_w}{k_2}}{v_w-\frac{u_w}{k_2}}}\right]\right\} \tag{C13}$$

Performance of the integration indicated in equation (C13) and the use of equations (A15) yields

$$(C_p)_{VII} = \frac{2\alpha}{B\pi}\frac{k_1+1}{\sqrt{k_1}}\cos^{-1}\frac{\left[\left(1+\frac{2k_1}{k_2}\right)(1-B\tan\beta)-k_1(1+B\tan\beta)\right]x-\left[\left(1+\frac{2k_1}{k_2}\right)(B+\tan\beta)+k_1(B-\tan\beta)\right]y}{\left[(1-B\tan\beta)+k_1(1+B\tan\beta)\right]x+\left[k_1(B-\tan\beta)-(B+\tan\beta)\right]y} +$$

$$\frac{4\alpha}{B\pi}\frac{k_2-1}{k_2}\sqrt{\frac{\left(1+\frac{k_1}{k_2}\right)(1-B\tan\beta)x-\left(1+\frac{k_1}{k_2}\right)(B+\tan\beta)y}{\left[(1+B\tan\beta)-\frac{1}{k_2}(1-B\tan\beta)\right]x+\left[(B-\tan\beta)+\frac{1}{k_2}(B+\tan\beta)\right]y}} -$$

$$\frac{4\alpha}{B\pi}\frac{k_1+1}{\sqrt{k_1}}\tan^{-1}\sqrt{\frac{(k_1+k_3)(1+B\tan\beta)x+(k_1+k_3)(B-\tan\beta)y-\frac{2Bk_3d}{M\cos\beta}}{\frac{2B}{\cos^2\beta(1+B\tan\beta)}\left(\frac{b}{2}-y\right)}} +$$

$$\frac{4\alpha}{B\pi}(1-k_3)\sqrt{\frac{\left(1+\frac{k_3}{k_1}\right)(1+B\tan\beta)x+\left(1+\frac{k_3}{k_1}\right)(B-\tan\beta)y-\frac{2Bk_3d}{Mk_1\cos\beta}}{\frac{2B}{\cos^2\beta(1+B\tan\beta)}\left(\frac{b}{2}-y\right)}} \tag{C14}$$

Region VIII.- Region VIII is the hatched portion of the wing shown below.

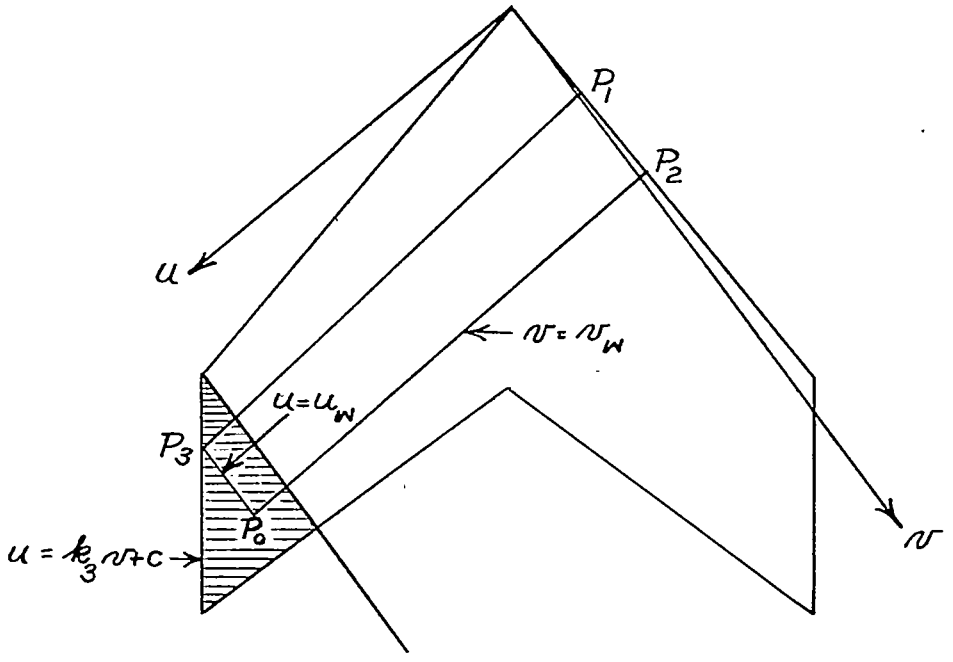

Point	u coordinate	v coordinate
P_0	u_w	v_w
P_1	$\frac{k_1(u_w - c)}{-k_3}$	$\frac{u_w - c}{k_3}$
P_2	$-k_1 v_w$	v_w
P_3	u_w	$\frac{u_w - c}{k_3}$

Region VIII is influenced by the wing tip on the left half-wing, which, because of the flow inclination caused by sideslip, has the characteristics of a subsonic trailing edge. Inasmuch as application of the Kutta-Joukowski condition at the tip is desired, equation (C2) must be used to obtain $f(u_w, v_w)$ for this region. Upon substitution of the appropriate limits and relations in equation (C6) the pressure coefficient in region VIII is given by

$$(C_p)_{VIII} = \frac{2\alpha}{B\pi} \int_{\frac{u_w - c}{k_3}}^{v_w} \frac{(k_1 + 1)dv}{\sqrt{(u_w + k_1 v)(v_w - v)}} \tag{C15}$$

Performance of the integration indicated in equation (C15) and application of equations (A15) yields

$$(C_p)_{VIII} = \frac{4\alpha}{B\pi} \frac{k_1 + 1}{\sqrt{k_1}} \tan^{-1} \sqrt{\frac{\frac{2k_1 B}{\cos^2\beta(1 - B\tan\beta)}\left(\frac{b}{2} + y\right)}{\left(1 + \frac{k_1}{k_3}\right)(1 - B\tan\beta)x - \left(1 + \frac{k_1}{k_3}\right)(B + \tan\beta)y - \frac{k_1 Bb}{\cos^2\beta(1 - B\tan\beta)}}} \tag{C16}$$

Region II. - The expression for the pressure distribution for region II (see fig. 7) has been derived in appendix A (eq. (A19)). For purposes of completeness, equation (A19) is given below in the notation used in this appendix.

$$(C_p)_{II} = \frac{4\alpha}{B\pi} \frac{k_2 - 1}{k_2} \sqrt{\frac{\frac{2B}{\cos^2\beta(1 + B\tan\beta)}\left(\frac{b}{2} - y\right)}{\left[(1 + B\tan\beta) - \frac{1}{k_2}(1 - B\tan\beta)\right]x + \left[(B - \tan\beta) + \frac{1}{k_2}(B + \tan\beta)\right]y}} + \frac{4\alpha}{B\pi}(1 - k_3)\sqrt{\frac{\left[(1 + B\tan\beta) - \frac{1}{k_2}(1 - B\tan\beta)\right]x + \left[(B - \tan\beta) + \frac{1}{k_2}(B + \tan\beta)\right]y}{\frac{2B}{\cos^2\beta(1 + B\tan\beta)}\left(\frac{b}{2} - y\right)}} \tag{C17}$$

APPENDIX D

DERIVATION OF EQUATIONS FOR THE PRESSURE DISTRIBUTION FOR WINGS WITH BOTH LEADING EDGES SUPERSONIC

Equations for the pressure distribution for wings with both leading edges supersonic are derived in this appendix. The plan form under consideration is shown in figure 8. The method used in appendix C for deriving the pressure formulas is also applied to this new class of wings. Actually, regions IV, VI, and VIII (see fig. 7) have already been treated in appendix C. The formulas for the pressure coefficients are given by equations (C8), (C12), and (C16). Corresponding results for the remaining wing regions are derived in this appendix by using equations (A15) of appendix A and equations (C2), (C3), and (C6) of appendix C.

Region IX.- Region IX is the hatched portion of the wing shown below.

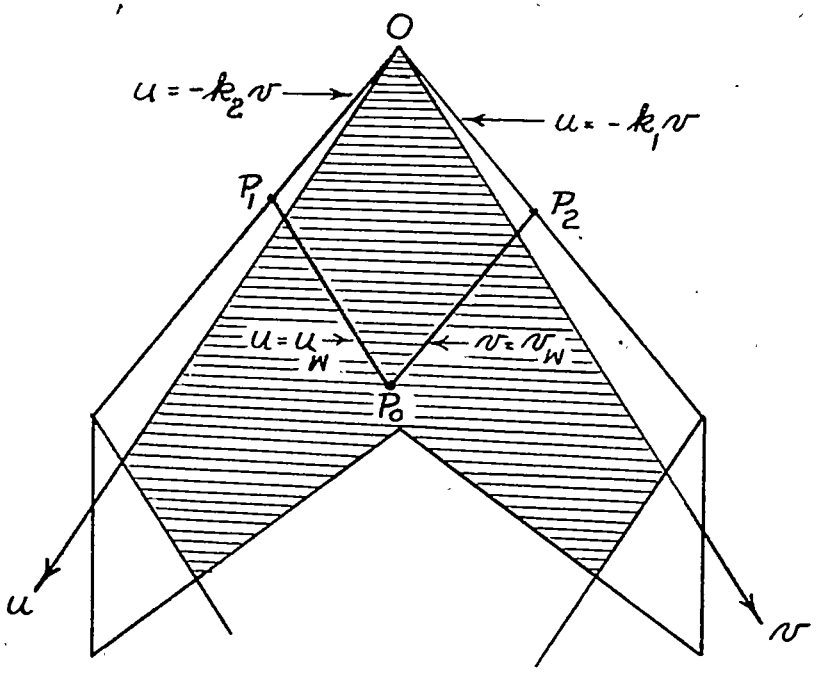

Point	u coordinate	v coordinate
0	0	0
P_0	u_w	v_w
P_1	u_w	$-u_w/k_2$
P_2	$-k_1 v_w$	v_w

Inasmuch as region IX is not influenced by either wing tip, equation (C2) gives the proper form of $f(u_w, v_w)$ for this region.

Substitution of proper limits and relations into equation (C6) gives the following equation for the pressure coefficient:

$$(C_p)_{IX} = 2\alpha\left[\frac{1}{B\pi}\int_0^{u_w} \frac{\frac{k_2 + 1}{k_2}\,du}{\sqrt{(u_w - u)\left(v_w + \frac{u}{k_2}\right)}} + \frac{1}{B\pi}\int_0^{v_w} \frac{(k_1 + 1)\,dv}{\sqrt{(u_w + k_1 v)(v_w - v)}}\right] \tag{D1}$$

Performance of the integration indicated in equation (D1) and application of equations (A15) yields

$$(C_p)_{IX} = \frac{2\alpha}{B\pi}\frac{k_2 + 1}{\sqrt{k_2}}\cos^{-1}\frac{\left[k_2(1 + B\tan\beta) - (1 - B\tan\beta)\right]x + \left[k_2(B - \tan\beta) + (B + \tan\beta)\right]y}{\left[k_2(1 + B\tan\beta) + (1 - B\tan\beta)\right]x + \left[k_2(B - \tan\beta) - (B + \tan\beta)\right]y} +$$

$$\frac{2\alpha}{B\pi}\frac{k_1 + 1}{\sqrt{k_1}}\cos^{-1}\frac{\left[(1 - B\tan\beta) - k_1(1 + B\tan\beta)\right]x - \left[(B + \tan\beta) + k_1(B - \tan\beta)\right]y}{\left[k_1(1 + B\tan\beta) + (1 - B\tan\beta)\right]x + \left[k_1(B - \tan\beta) - (B + \tan\beta)\right]y} \tag{D2}$$

Region X.- Region X is the hatched portion of the wing shown below.

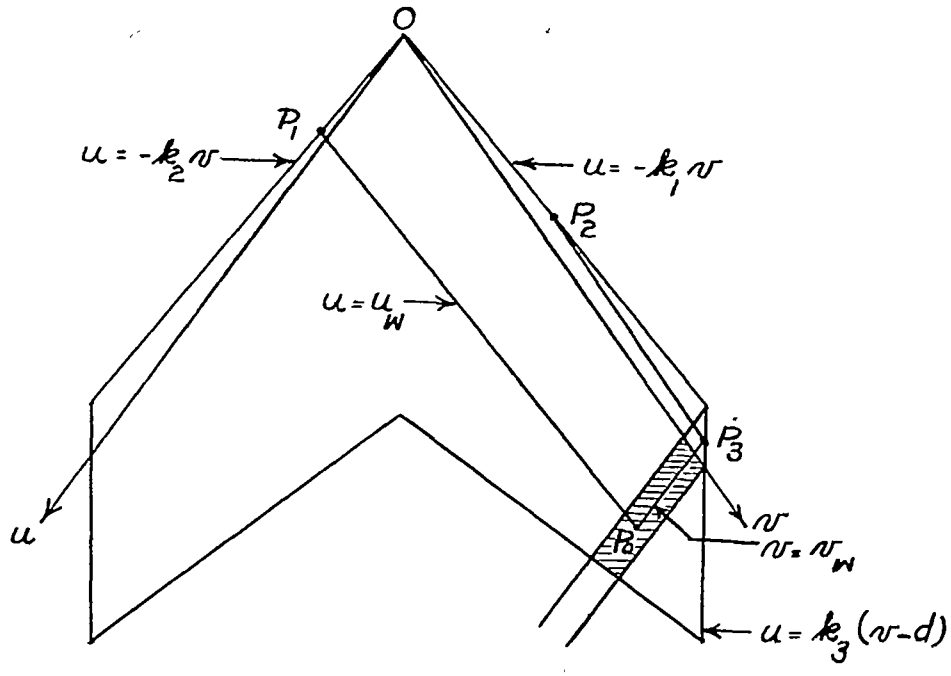

Point	u coordinate	v coordinate
O	0	0
P_0	u_w	v_w
P_1	u_w	$-u_w/k_2$
P_2	$k_3(v_w - d)$	$-\frac{k_3(v_w - d)}{k_1}$
P_3	$k_3(v_w - d)$	v_w

Since region X is influenced by the right wing tip, the proper value of $f(u_w, v_w)$ is given by equation (C3). Substituting the appropriate

limits and relations into equation (C6) gives the following equation for the pressure coefficient in region X:

$$(C_p)_X = \frac{2\alpha}{B\pi}\int_0^{u_w} \frac{\frac{k_2+1}{k_2}\,du}{\sqrt{(u_w-u)\left(v_w+\frac{u}{k_2}\right)}} + \frac{2\alpha}{B\pi}\int_0^{\frac{-(v_w-d)k_3}{k_1}} \frac{(k_1+1)dv}{\sqrt{(u_w+k_1v)(v_w-v)}} +$$

$$\frac{4\alpha}{B\pi}(1-k_3)\sqrt{\frac{v_w+k_3\frac{v_w-d}{k_1}}{u_w-k_3(v_w-d)}} \qquad (D3)$$

Performance of the integration indicated in equation (D3) and application of equations (A15) yields

$$(C_p)_X = \frac{2\alpha}{B\pi}\frac{k_2+1}{\sqrt{k_2}}\cos^{-1}\frac{\left[k_2(1+B\tan\beta)-(1-B\tan\beta)\right]x+\left[k_2(B-\tan\beta)+(B+\tan\beta)\right]y}{\left[k_2(1+B\tan\beta)+(1-B\tan\beta)\right]x+\left[k_2(B-\tan\beta)-(B+\tan\beta)\right]y} +$$

$$\frac{2\alpha}{B\pi}\frac{k_1+1}{\sqrt{k_1}}\cos^{-1}\frac{\left[(1-B\tan\beta)-k_1(1+B\tan\beta)\right]x-\left[B+\tan\beta+k_1(B-\tan\beta)\right]y}{\left[k_1(1+B\tan\beta)+(1-B\tan\beta)\right]x+\left[k_1(B-\tan\beta)-(B+\tan\beta)\right]y} -$$

$$\frac{4\alpha}{B\pi}\frac{k_1+1}{\sqrt{k_1}}\tan^{-1}\sqrt{\frac{(k_1+k_3)(1+B\tan\beta)x+(k_1+k_3)(B-\tan\beta)y-\frac{Bb}{\cos^2\beta(1+B\tan\beta)}}{\frac{2B}{\cos^2\beta(1+B\tan\beta)}\left(\frac{b}{2}-y\right)}} +$$

$$\frac{4\alpha}{B\pi}(1-k_3)\sqrt{\frac{\left(1+\frac{k_3}{k_1}\right)(1+B\tan\beta)x+\left(1+\frac{k_3}{k_1}\right)(B-\tan\beta)y-\frac{Bb}{k_1\cos^2\beta(1+B\tan\beta)}}{\frac{2B}{\cos^2\beta(1+B\tan\beta)}\left(\frac{b}{2}-y\right)}} \qquad (D4)$$

Region XI.- Region XI is the hatched portion of the wing shown below.

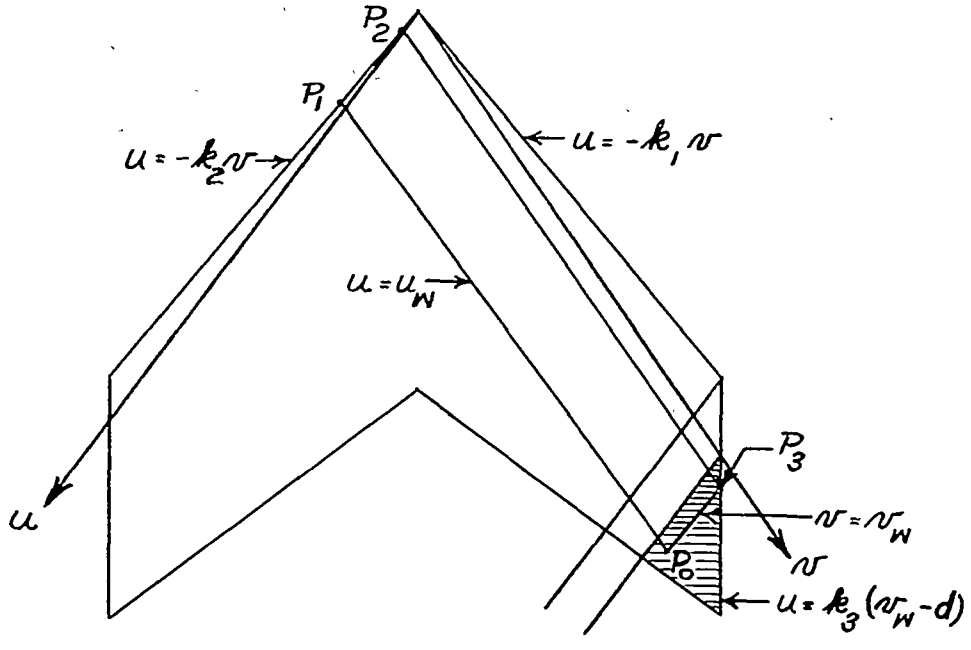

Point	u coordinate	v coordinate
P_0	u_w	v_w
P_1	u_w	$-u_w/k_2$
P_2	$k_3(v_w - d)$	$-\frac{k_3(v_w - d)}{k_2}$
P_3	$k_3(v_w - d)$	v_w

As region XI is influenced by the wing tip on the right half-wing, the correct form of $f(u_w, v_w)$ is given by equation (C3). Substitution of

the proper limits and relation into equation (C6) gives the following equation for the pressure coefficient in region XI:

$$(C_p)_{XI} = \frac{2\alpha}{B\pi}\int_{k_3(v_w-d)}^{u_w} \frac{\frac{k_2+1}{k_2}\,du}{\sqrt{(u_w-u)\left(v_w+\frac{u}{k_2}\right)}} + \frac{4\alpha}{B\pi}(1-k_3)\sqrt{\frac{v_w+\frac{k_3(v_w-d)}{k_2}}{u_w-k_3(v_w-d)}} \qquad (D5)$$

Performance of the integration indicated in equation (D5) and application of equations (A15) yields

$$(C_p)_{XI} = \frac{2\alpha}{B}\frac{k_2+1}{\sqrt{k_2}}\left\{1-\frac{1}{\pi}\cos^{-1}\frac{\left[(1-B\tan\beta)+k_2(1+B\tan\beta)\right]x-\left[(B+\tan\beta)+(k_2+2k_3)(B-\tan\beta)\right]y+\frac{2Bb}{\cos^2\beta(1+B\tan\beta)}}{\left[k_2(1+B\tan\beta)+1-B\tan\beta\right]x+\left[k_2(B-\tan\beta)-(B+\tan\beta)\right]y}\right\}+$$

$$\frac{4\alpha}{B\pi}(1-k_3)\sqrt{\frac{\left(1+\frac{k_3}{k_2}\right)(1+B\tan\beta)x+\left(1+\frac{k_3}{k_2}\right)(B-\tan\beta)y-\frac{Bb}{k_2\cos^2\beta(1+B\tan\beta)}}{\frac{2B}{(1+B\tan\beta)\cos^2\beta}\left(\frac{b}{2}-y\right)}} \qquad (D6)$$

Region XII.- Region XII is the hatched portion of the wing shown below.

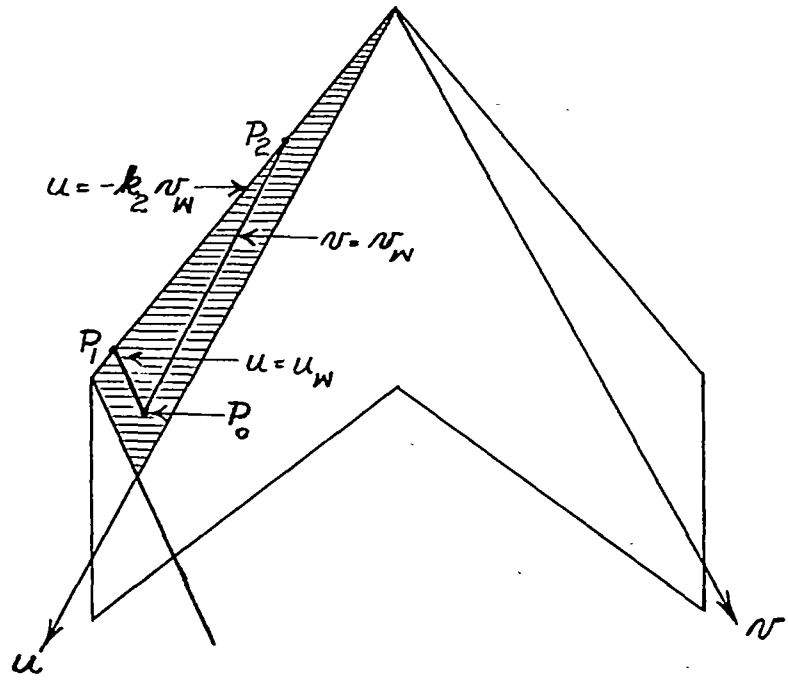

Point	u coordinate	v coordinate
P_0	u_w	v_w
P_1	u_w	$-u_w/k_2$
P_2	$-k_2 v_w$	v_w

Inasmuch as region XII is not influenced by either the right or left wing tip, equation (C2) gives the correct value for $f(u_w, v_w)$. The proper substitutions of limits and relations into equation (C6) give the following equation for the pressure coefficient in region XII:

$$(C_p)_{XII} = \frac{2\alpha}{k_2 B\pi} \int_{-k_2 v_w}^{u_w} \frac{(k_2 + 1)\,du}{\sqrt{(u_w - u)\left(v_w + \frac{u}{k_2}\right)}} \tag{D7}$$

Performance of the integration indicated in equation (D7) yields

$$(C_p)_{XII} = \frac{2\alpha}{B} \frac{k_2 + 1}{\sqrt{k_2}} \tag{D8}$$

Region XIII.- Region XIII is the hatched portion of the wing shown below.

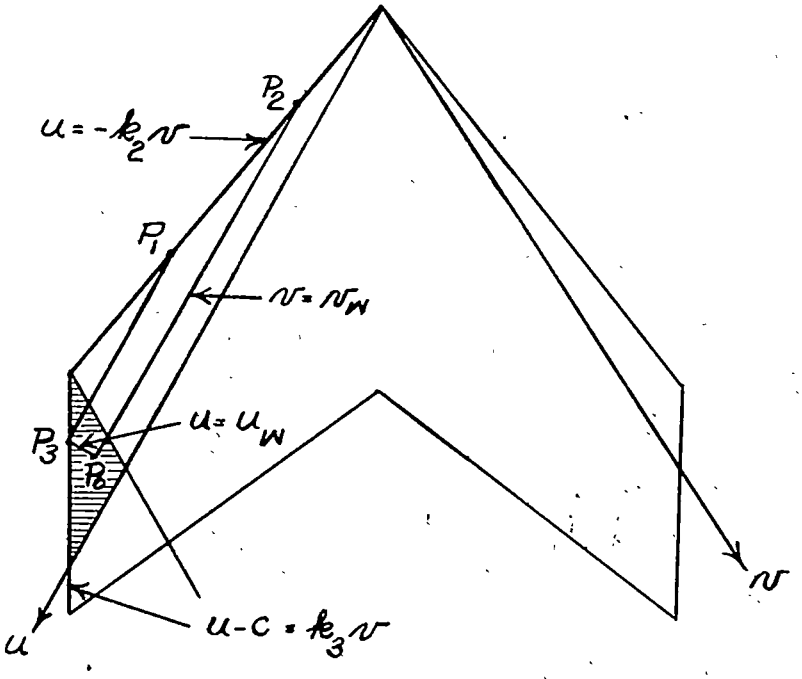

Point	u coordinate	v coordinate
P_0	u_w	v_w
P_1	$-\frac{k_2(u_w - c)}{k_3}$	$\frac{u_w - c}{k_3}$
P_2	$-k_2 v_w$	v_w
P_3	u_w	$\frac{u_w - c}{k_3}$

Region XIII is influenced by the left wing tip which, because of the asymmetric flow caused by the sideslip, has the characteristics of a subsonic trailing edge. Inasmuch as the Kutta-Joukowski condition is to be satisfied at this tip, the correct form of $f(u_w, v_w)$ is given by equation (C2).

The substitution of appropriate limits and relations into equation (C6) gives the following equation for the pressure coefficient in region XIII:

$$(C_p)_{XIII} = 4\alpha \frac{1}{2B\pi} \int_{v_w}^{\frac{u_w - c}{k_3}} \frac{(k_2 + 1)dv}{\sqrt{(u_w + k_2 v)(v_w - v)}} \tag{D9}$$

Performance of the integration indicated in equation (D9) and the application of equations (A15) yields

$$(C_p)_{XIII} = \frac{2\alpha}{B} \frac{k_2 + 1}{\sqrt{k_2}} \left[1 - \frac{2}{\pi} \tan^{-1} \sqrt{\frac{\left(1 + \frac{k_2}{k_3}\right)(1 - B \tan \beta)x - \left(1 + \frac{k_2}{k_3}\right)(B + \tan \beta)y - \frac{k_2 B b}{\cos^2 \beta (1 - B \tan \beta)}}{\frac{2Bk_2}{\cos^2 \beta (1 - B \tan \beta)} \left(\frac{b}{2} + y\right)}} \right] \tag{D10}$$

Region XIV.- Region XIV is the hatched portion of the wing shown below.

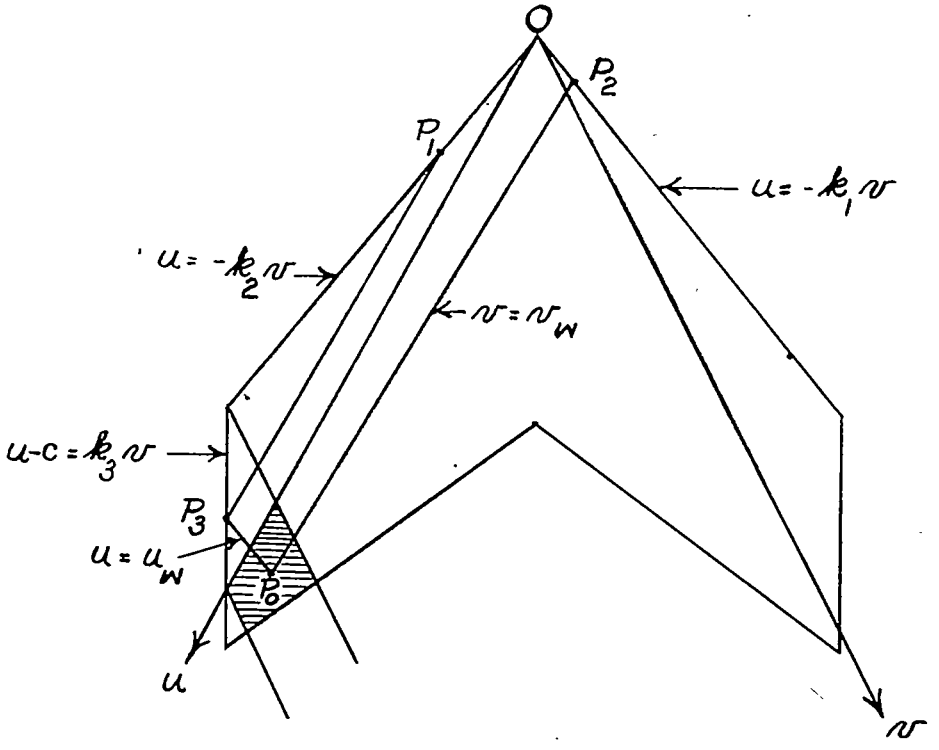

Point	u coordinate	v coordinate
0	0	0
P_0	u_w	v_w
P_1	$-\frac{k_2(u_w - c)}{k_3}$	$\frac{u_w - c}{k_3}$
P_2	$-k_1 v_w$	v_w
P_3	u_w	$\frac{u_w - c}{k_3}$

Region XIV is influenced by the left wing tip. Inasmuch as the Kutta-Joukowski condition is imposed at this tip, equation (C2) gives the correct form of $f(u_w, v_w)$. Substitution of the proper limits and relations into equation (C6) gives for the pressure coefficient in region XIV.

$$(C_p)_{XIV} = \frac{2\alpha}{B\pi}\left[\int_0^{\frac{u_w - c}{k_3}} \frac{(k_2 + 1)dv}{\sqrt{(u_w + k_2 v)(v_w - v)}} + \int_0^{v_w} \frac{(k_1 + 1)dv}{\sqrt{(u_w + k_1 v)(v_w - v)}}\right] \tag{D11}$$

Performance of the integration indicated in equation (D11) and application of equations (A15) yields

$$(C_p)_{XIV} = \frac{2\alpha}{B\pi}\frac{k_2 + 1}{\sqrt{k_2}}\cos^{-1}\frac{\left[k_2(1 + B\tan\beta) - (1 - B\tan\beta)\right]x + \left[k_2(B - \tan\beta) + (B + \tan\beta)\right]y}{\left[k_2(1 + B\tan\beta) + (1 - B\tan\beta)\right]x + \left[k_2(B - \tan\beta) - (B + \tan\beta)\right]y} +$$

$$\frac{2\alpha}{B\pi}\frac{k_1 + 1}{\sqrt{k_1}}\cos^{-1}\frac{\left[(1 - B\tan\beta) - k_1(1 + B\tan\beta)\right]x - \left[(B + \tan\beta) + k_1(B - \tan\beta)\right]y}{\left[k_1(1 + B\tan\beta) + (1 - B\tan\beta)\right]x + \left[k_1(B - \tan\beta) + (B + \tan\beta)\right]y} -$$

$$\frac{4\alpha}{B\pi}\frac{k_2 + 1}{\sqrt{k_2}}\tan^{-1}\sqrt{\frac{\left(1 + \frac{k_2}{k_3}\right)(1 - B\tan\beta)x - \left(1 + \frac{k_2}{k_3}\right)(B + \tan\beta)y - \frac{k_2 bB}{\cos^2\beta(1 - B\tan\beta)}}{\frac{2k_2 B}{\cos^2\beta(1 - B\tan\beta)}\left(\frac{b}{2} + y\right)}} \tag{D12}$$

REFERENCES

1. Ribner, Herbert S.: The Stability Derivatives of Low-Aspect-Ratio Triangular Wings at Subsonic and Supersonic Speeds. NACA TN 1423, 1947.

2. Jones, Arthur L., and Alksne, Alberta: The Damping Due to Roll of Triangular, Trapezoidal, and Related Plan Forms in Supersonic Flow. NACA TN 1548, 1948.

3. Jones, Arthur L., Spreiter, John R., and Alksne, Alberta: The Rolling Moment Due To Sideslip of Triangular, Trapezoidal, and Related Plan Forms in Supersonic Flow. NACA TN 1700, 1948.

4. Ribner, Herbert S., and Malvestuto, Frank S., Jr.: Stability Derivatives of Triangular Wings at Supersonic Speeds. NACA Rep. 908, 1948. (Supersedes NACA TN 1572.)

5. Malvestuto, Frank S., Jr., and Margolis, Kenneth: Theoretical Stability Derivatives of Thin Sweptback Wings Tapered to a Point With Sweptback or Sweptforward Trailing Edges for a Limited Range of Supersonic Speeds. NACA Rep. 971, 1950. (Supersedes NACA TN 1761.)

6. Harmon, Sidney M.: Stability Derivatives at Supersonic Speeds of Thin Rectangular Wings With Diagonals Ahead of Tip Mach Lines. NACA Rep. 925, 1949. (Supersedes NACA TN 1706.)

7. Jones, Arthur L., and Alksne, Alberta: The Yawing Moment Due to Sideslip of Triangular, Trapezoidal, and Related Plan Forms in Supersonic Flow. NACA TN 1850, 1949.

8. Brown, Clinton E., and Adams, Mac. C.: Damping in Pitch and Roll of Triangular Wings at Supersonic Speeds. NACA Rep. 892, 1948. (Supersedes NACA TN 1566.)

9. Margolis, Kenneth: Theoretical Lift and Damping in Roll of Thin Sweptback Tapered Wings With Raked-In and Cross-Stream Wing Tips at Supersonic Speeds. Subsonic Leading Edges. NACA TN 2048, 1950.

10. Jones, Arthur L.: The Theoretical Lateral-Stability Derivatives for Wings at Supersonic Speeds. Jour. Aero. Sci., vol. 17, no. 1, Jan. 1950, pp. 39-46.

11. Malvestuto, Frank S., Jr., Margolis, Kenneth, and Ribner, Herbert S.: Theoretical Lift and Damping in Roll at Supersonic Speeds of Thin Sweptback Tapered Wings With Streamwise Tips, Subsonic Leading Edges, and Supersonic Trailing Edges. NACA Rep. 970, 1950. (Supersedes NACA TN 1860.)

12. Harmon, Sidney M., and Jeffreys, Isabella: Theoretical Lift and Damping in Roll of Thin Wings With Arbitrary Sweep and Taper at Supersonic Speeds. Supersonic Leading and Trailing Edges. NACA TN 2114, 1950.

13. Cohen, Doris: The Theoretical Lift of Flat Swept-Back Wings at Supersonic Speeds. NACA TN 1555, 1948.

14. Cohen, Doris: Theoretical Loading at Supersonic Speeds of Flat Swept-Back Wings With Interacting Trailing and Leading Edges. NACA TN 1991, 1949.

15. Cohen, Doris: Formulas and Charts for the Supersonic Lift and Drag of Flat Swept-Back Wings With Interacting Leading and Trailing Edges. NACA TN 2093, 1950.

16. Walker, Harold J., and Ballantyne, Mary B.: Pressure Distribution and Damping in Steady Roll at Supersonic Mach Numbers of Flat Swept-Back Wings With Subsonic Edges. NACA TN 2047, 1950.

17. Ribner, Herbert S.: On the Effect of Subsonic Trailing Edges on Damping in Roll and Pitch of Thin Sweptback Wings in a Supersonic Stream. NACA TN 2146, 1950.

18. Malvestuto, Frank S., Jr., and Hoover, Dorothy M.: Lift and Pitching Derivatives of Thin Sweptback Tapered Wings With Streamwise Tips and Subsonic Leading Edges at Supersonic Speeds. NACA TN 2294, 1951.

19. Walker, Harold J., and Ballantyne, Mary B.: Pressure Distribution and Damping in Steady Pitch at Supersonic Mach Numbers of Flat Swept-Back Wings Having All Edges Subsonic. NACA TN 2197, 1950.

20. Martin, John C., Margolis, Kenneth, and Jeffreys, Isabella: Calculation of Lift and Pitching Moments Due to Angle of Attack and Steady Pitching Velocity at Supersonic Speeds for Thin Sweptback Tapered Wings With Streamwise Tips and Supersonic Leading and Trailing Edges. NACA TN 2699, 1952.

21. Malvestuto, Frank S., Jr., and Hoover, Dorothy M.: Supersonic Lift and Pitching Moment of Thin Sweptback Tapered Wings Produced by Constant Vertical Acceleration. Subsonic Leading Edges and Supersonic Trailing Edges. NACA TN 2315, 1951.

22. Margolis, Kenneth: Theoretical Calculations of the Lateral Force and Yawing Moment Due to Rolling at Supersonic Speeds for Swept-back Tapered Wings With Streamwise Tips. Subsonic Leading Edges. NACA TN 2122, 1950.

23. Harmon, Sidney M., and Martin, John C.: Theoretical Calculations of the Lateral Force and Yawing Moment Due to Rolling at Supersonic Speeds for Sweptback Tapered Wings With Streamwise Tips. Supersonic Leading Edges. NACA TN 2156, 1950.

24. Lampert, Seymour: Rolling and Yawing Moments for Swept-Back Wings in Sideslip at Supersonic Speeds. NACA TN 2262, 1951.

25. Evvard, John C.: Distribution of Wave Drag and Lift in the Vicinity of Wing Tips at Supersonic Speeds. NACA TN 1382, 1947.

26. Evvard, John C.: Theoretical Distribution of Lift on Thin Wings at Supersonic Speeds (An Extension). NACA TN 1585, 1948.

TABLE I

INDEX TO PRESSURE COEFFICIENTS FOR

VARIOUS WING REGIONS

Wing region[1]	Equation for C_p	Page
I	(A5)	13
II	(A19), (C17)	16,39
III	(A26)	18
IV	(C8)	32
V	(C10)	33
VI	(C12)	35
VII	(C14)	37
VIII	(C16)	39
IX	(D2)	41
X	(D4)	43
XI	(D6)	45
XII	(D8)	47
XIII	(D10)	48
XIV	(D12)	50

[1]Wing regions are identified in figures 4, 7, 8, and 9.

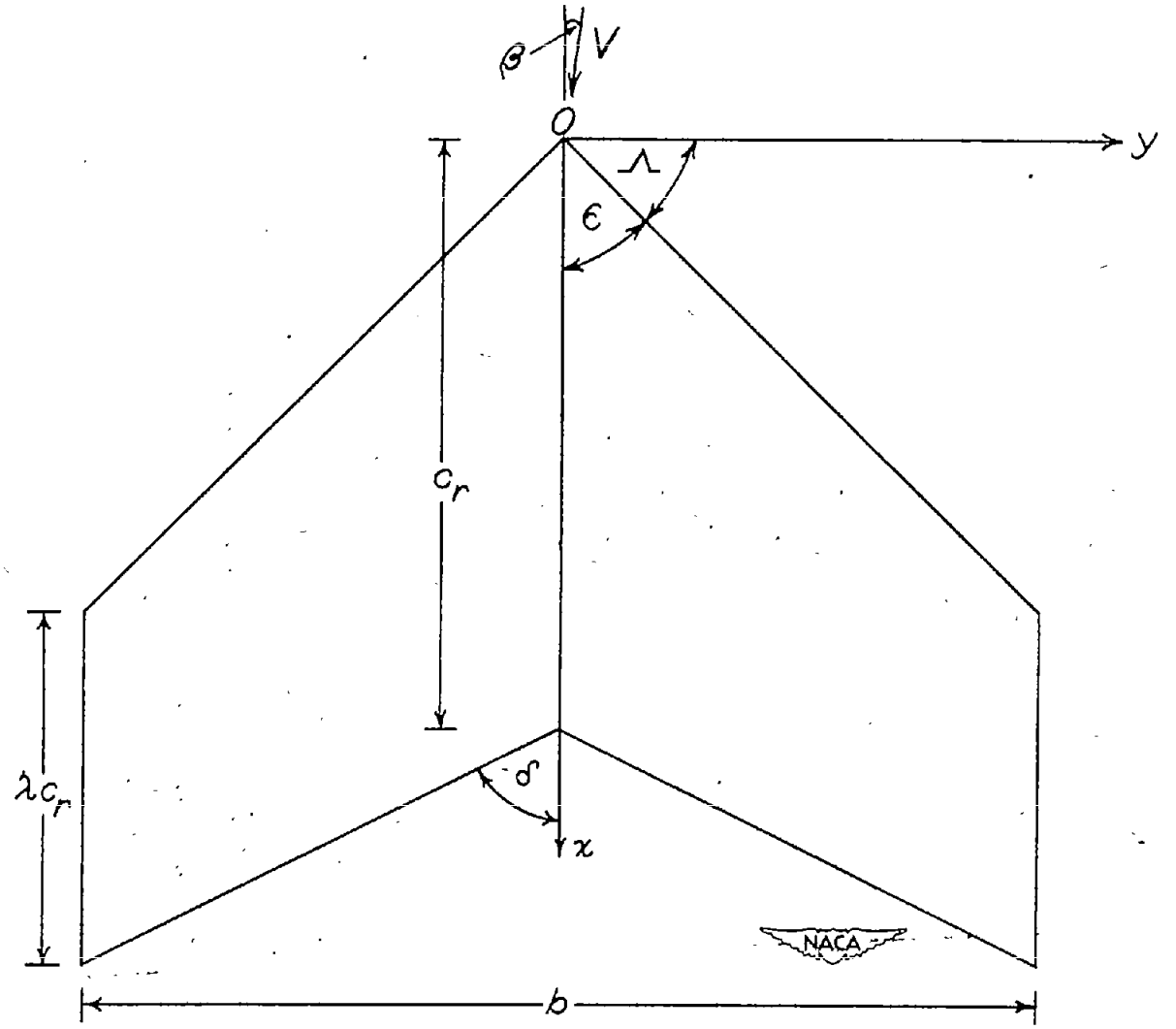

Figure 1.- Symbols and pertinent data associated with general wing plan form.

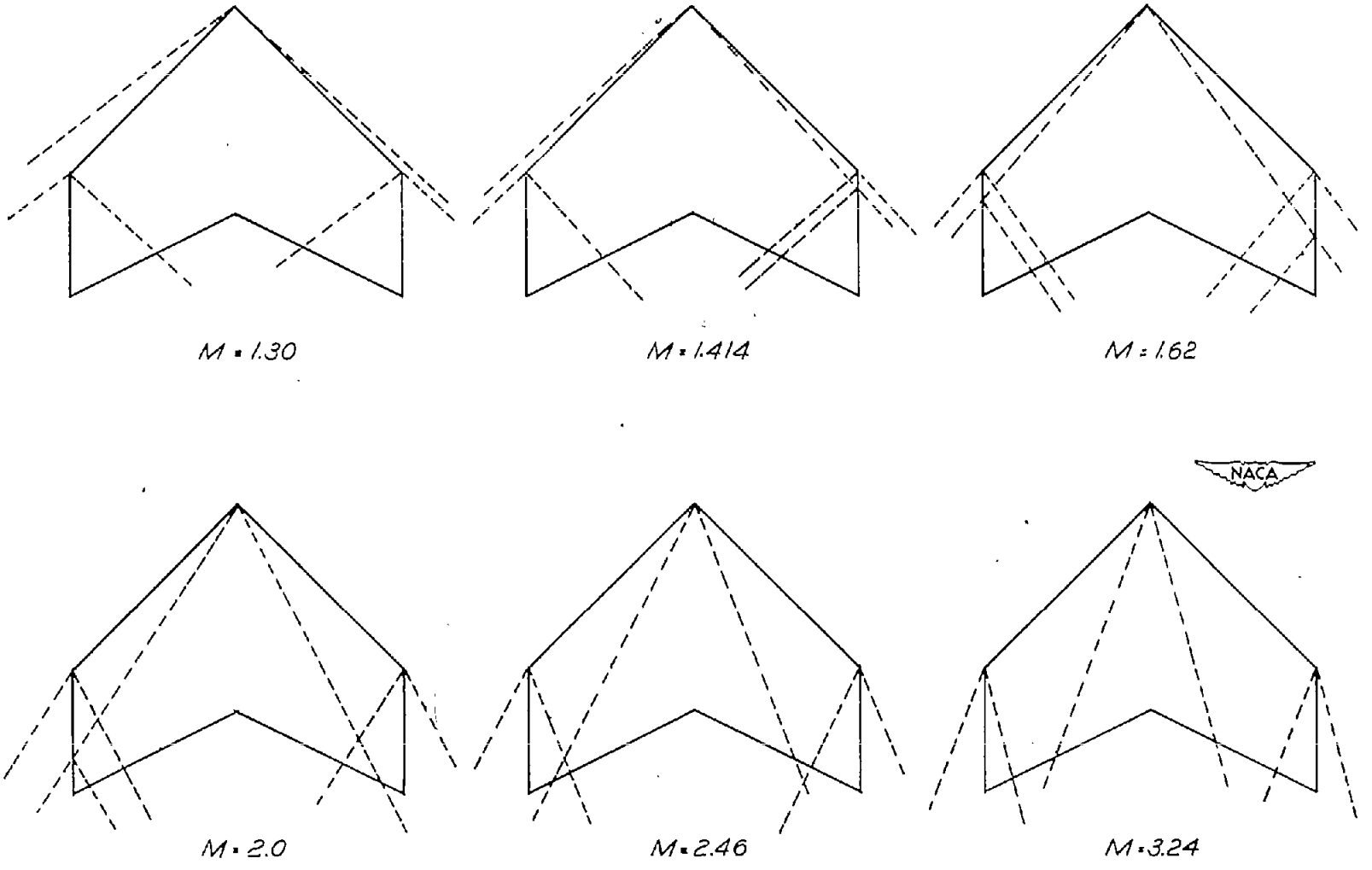

Figure 2.- Effect of Mach number on the Mach line–plan-form configuration for a given wing with an angle of sideslip of 3°. Dashed lines are Mach lines.

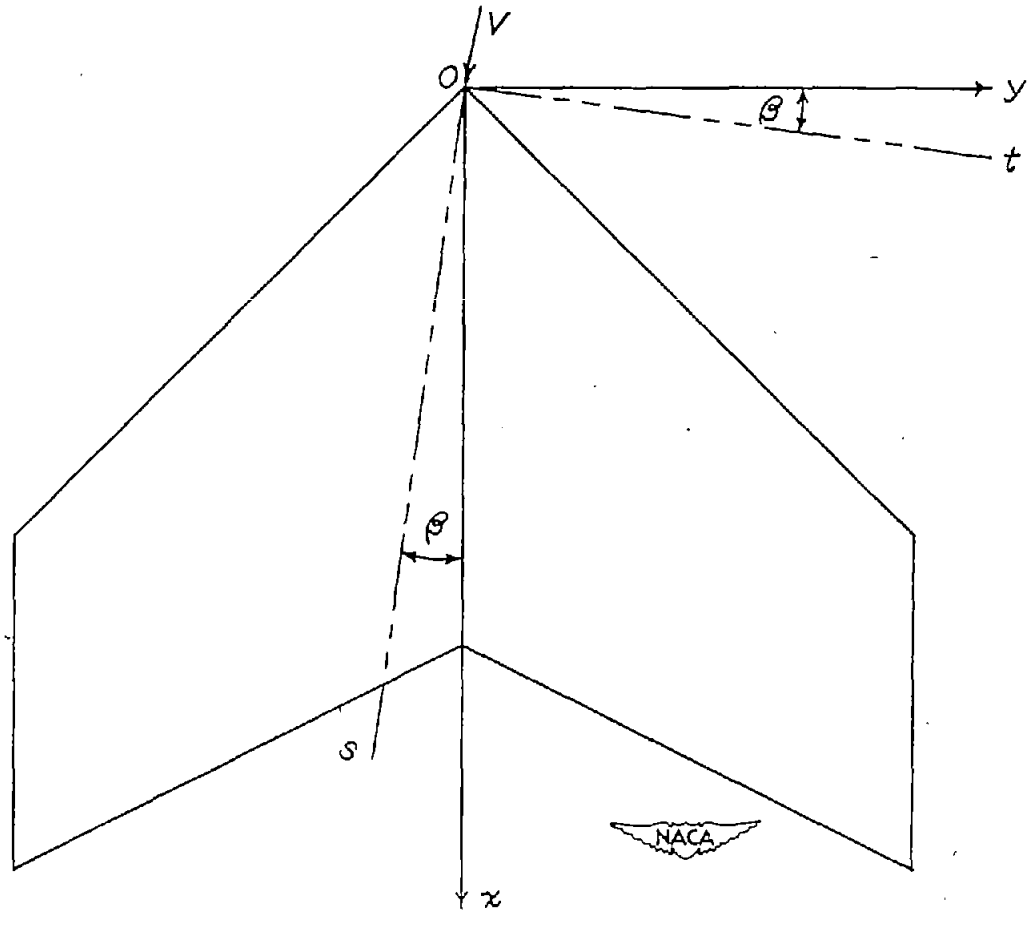

Figure 3.- Relationship between the s,t wind-axes system and the x,y body-axes system. $s = x \cos \beta - y \sin \beta$; $t = x \sin \beta + y \cos \beta$; $x = s \cos \beta + t \sin \beta$; $y = -s \sin \beta + t \cos \beta$.

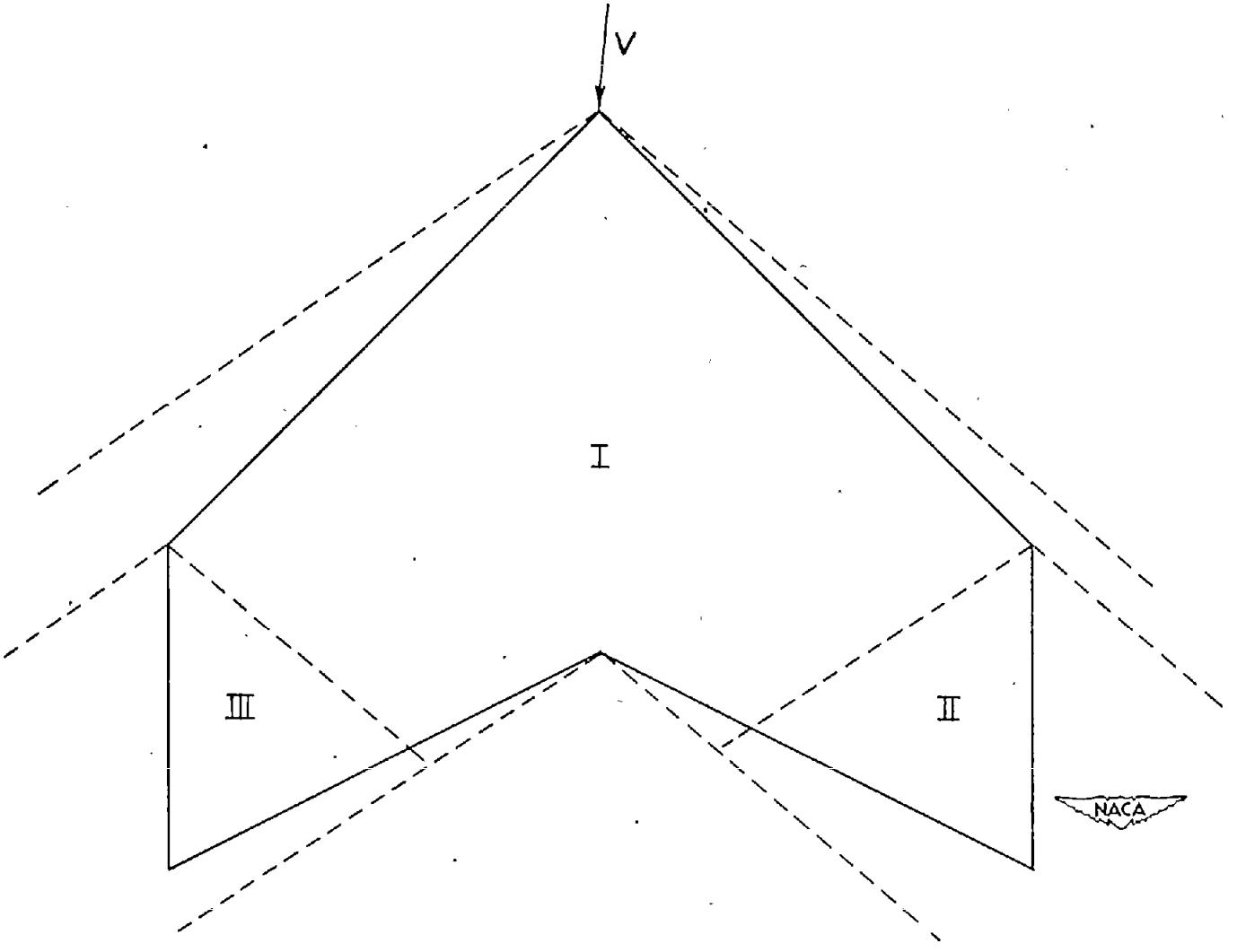

Figure 4.- Wing regions for the plan form with both leading edges subsonic. Dashed lines are Mach lines.

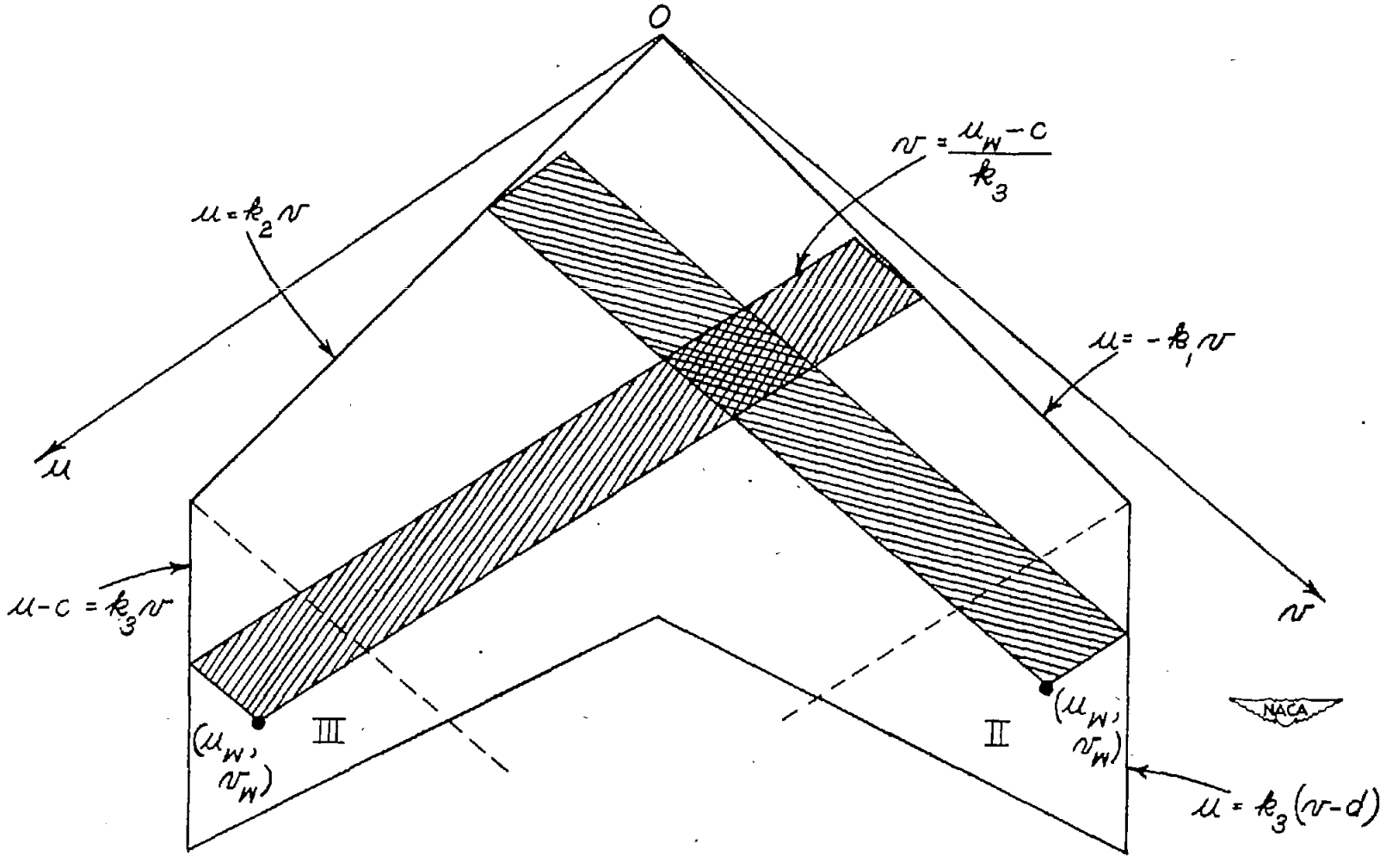

Figure 5.- Information pertinent to the derivation of the potentials for wing regions II and III. (See appendix A.)

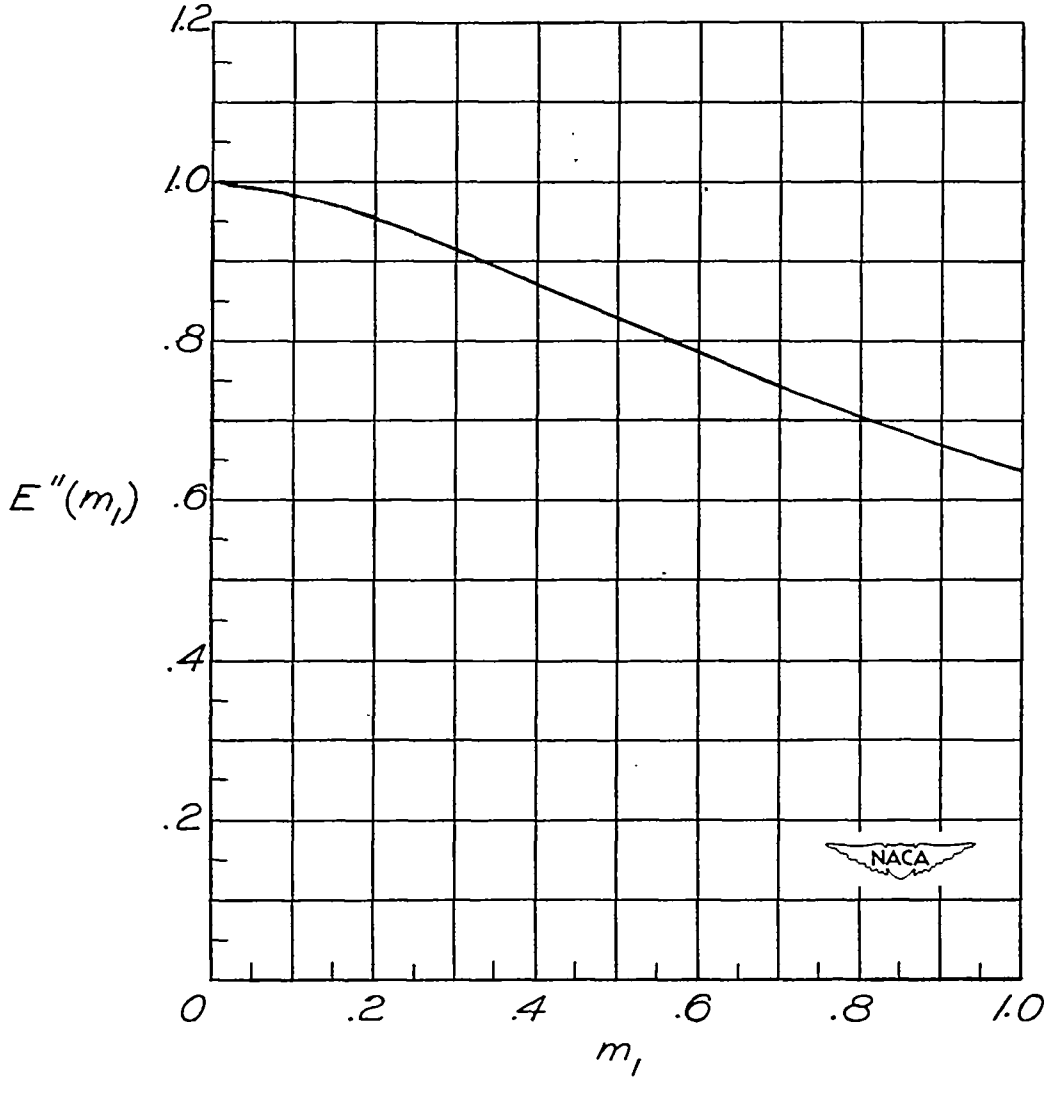

Figure 6.- Variation of the elliptic function $E''(m_1)$ with m_1.

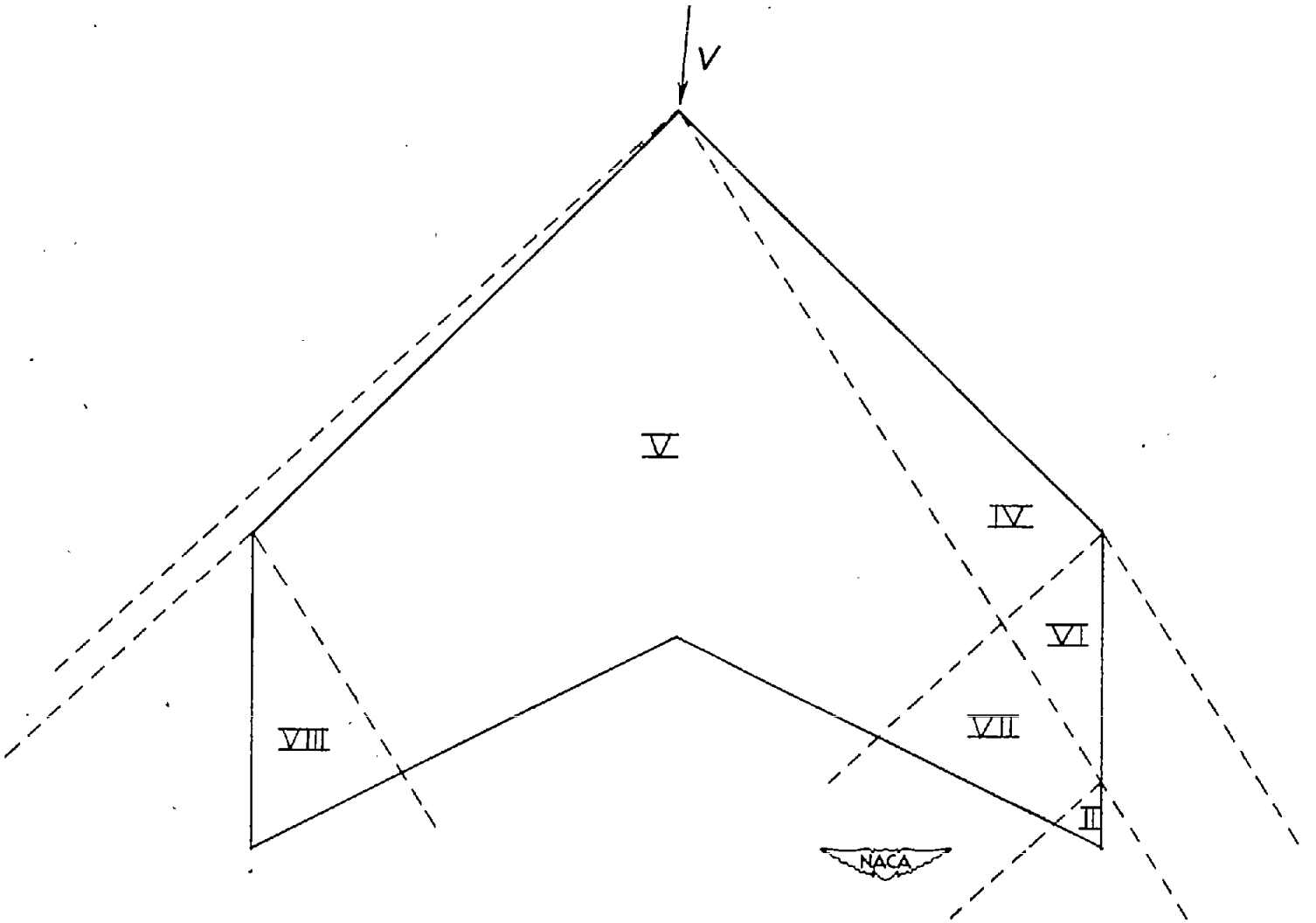

Figure 7.- Wing regions for the plan form with one leading edge subsonic and one leading edge supersonic. Dashed lines are Mach lines.

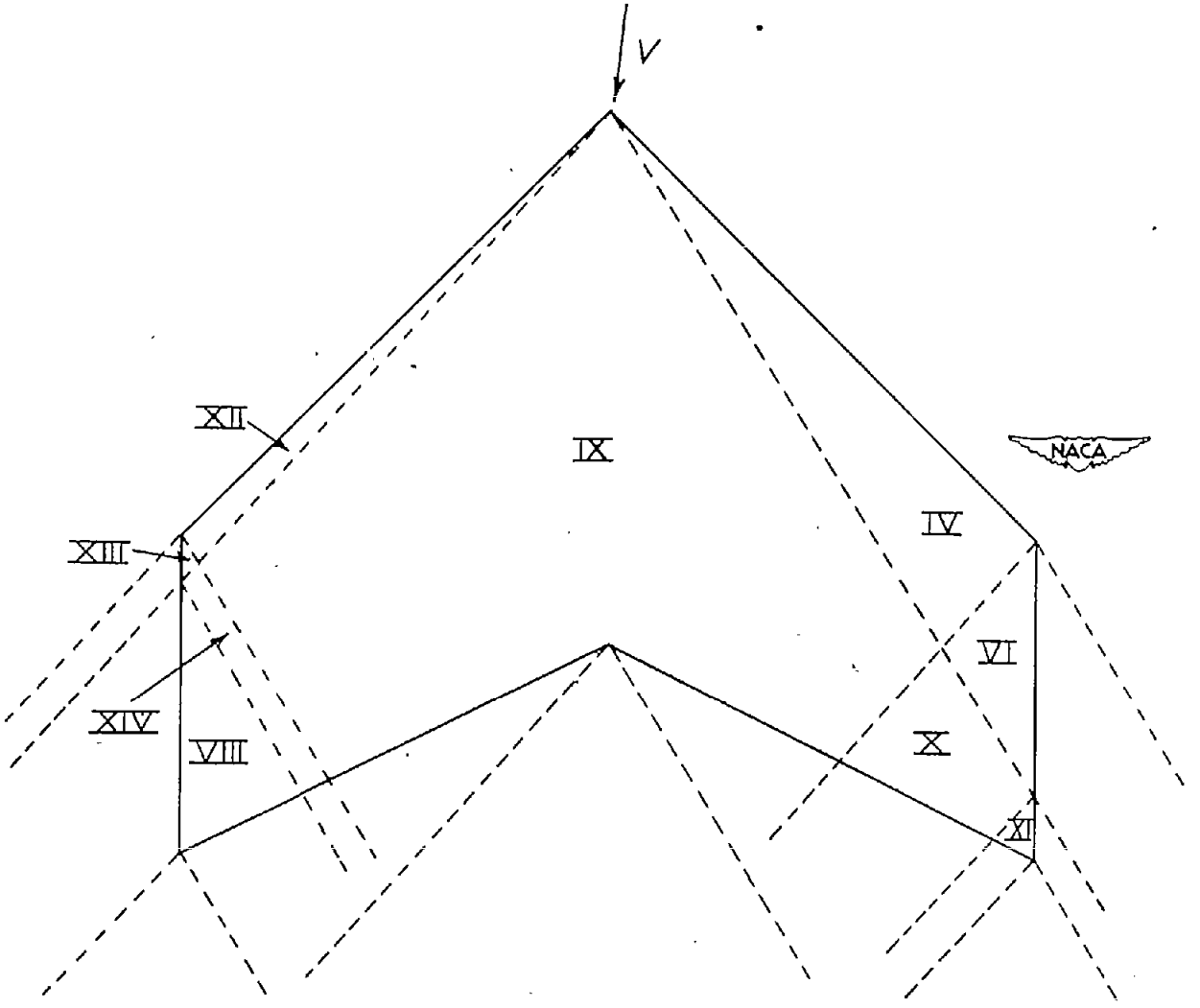

Figure 8.- Wing regions for the plan form with both leading edges supersonic. Dashed lines are Mach lines.

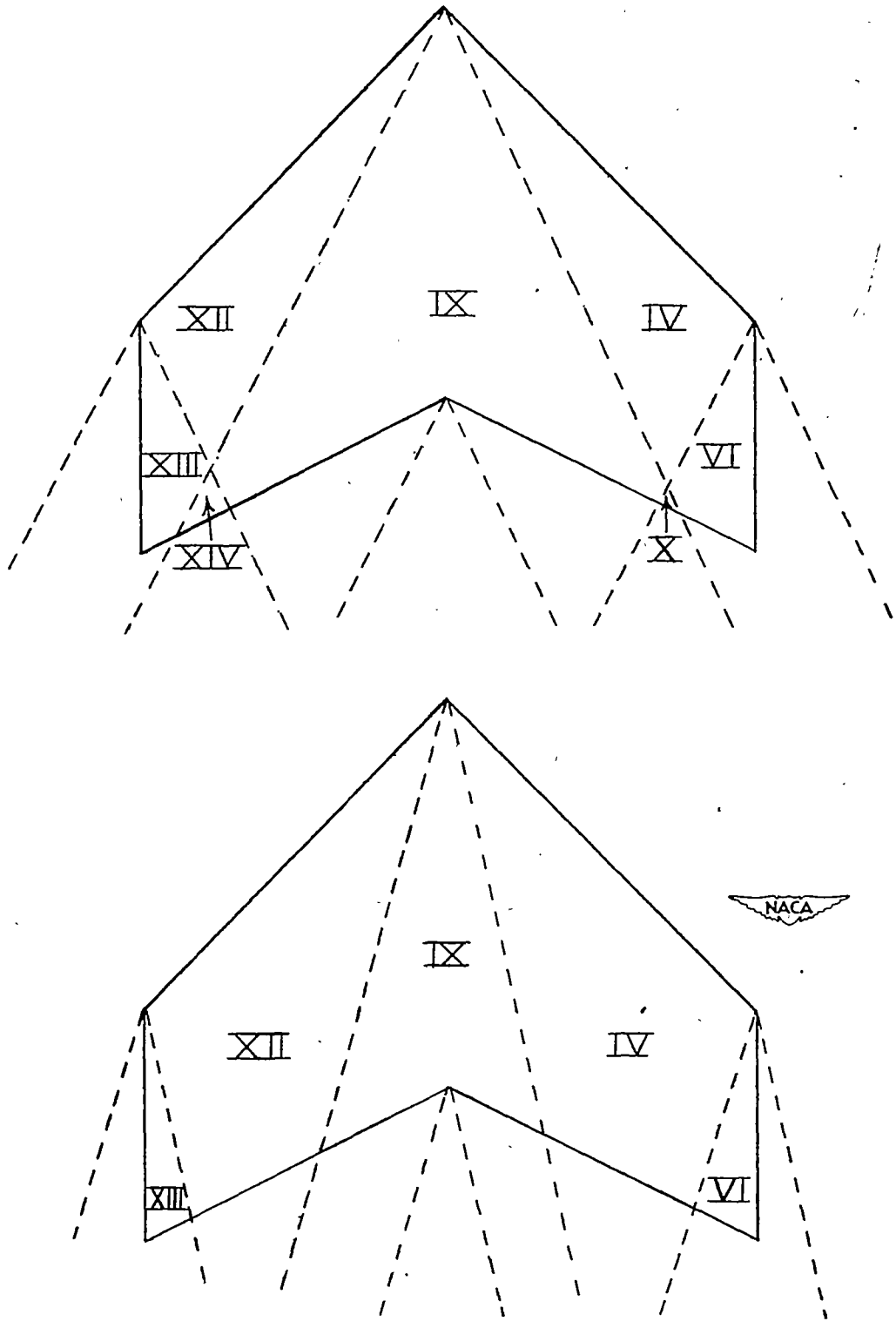

Figure 9.- Wing regions for some additional Mach line–plan-form configurations. Dashed lines are Mach lines.

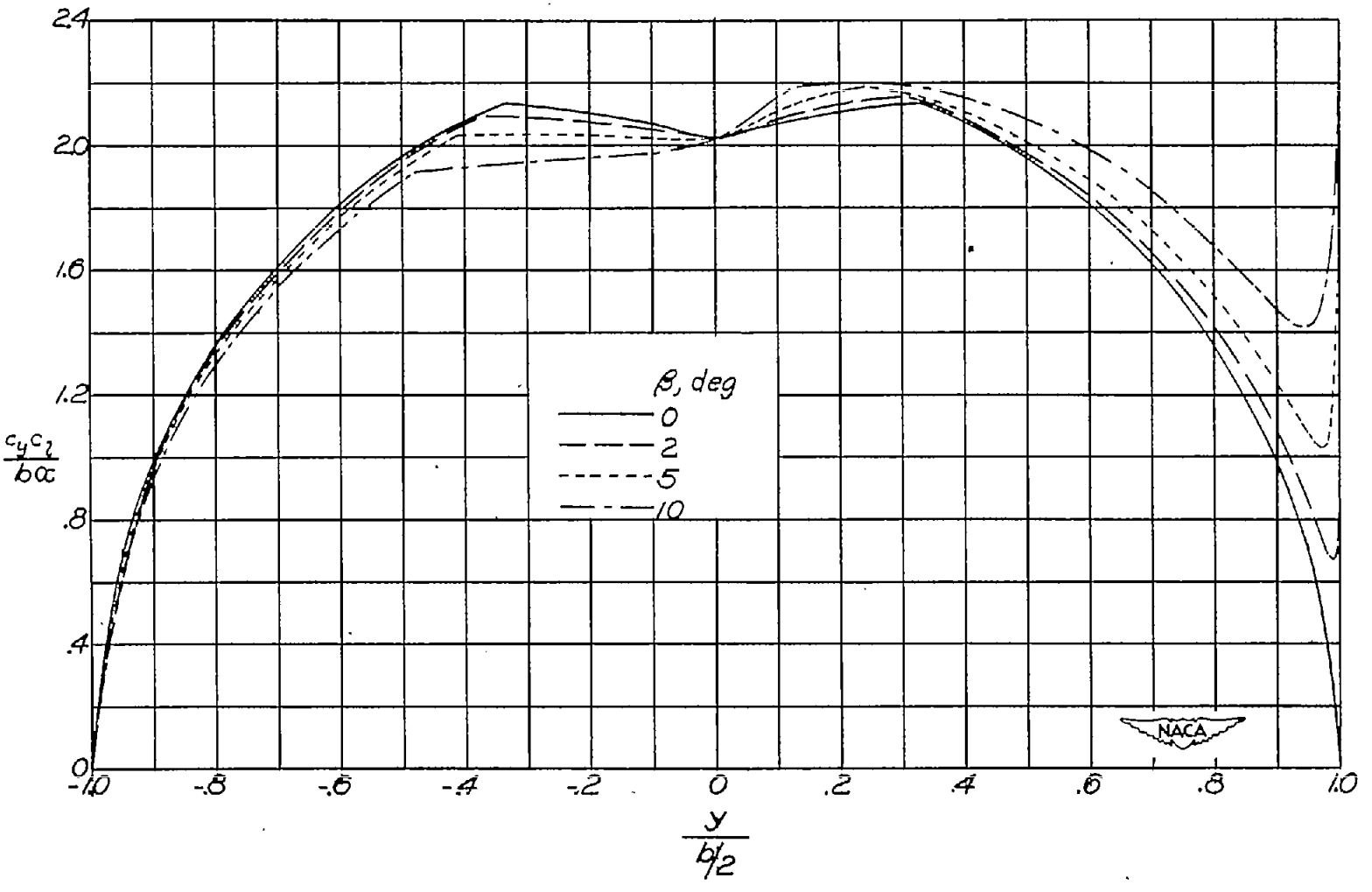

Figure 10.- Illustrative span loadings for various sideslip angles. Aspect ratio, 2; leading-edge sweepback, 45°; taper ratio, 0.50; Mach number, 1.2.

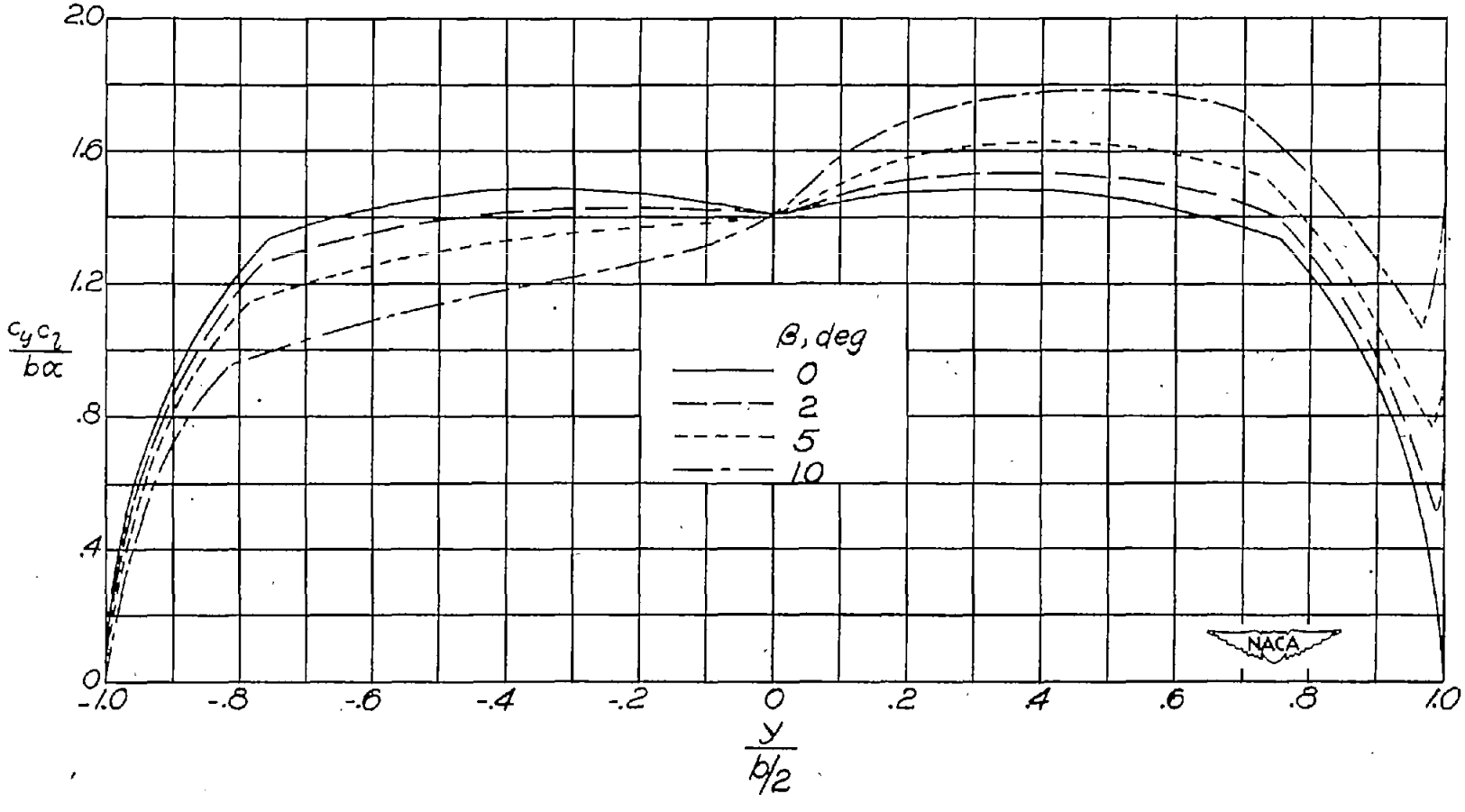

Figure 11.- Illustrative span loadings for various sideslip angles. Aspect ratio, 2; leading-edge sweepback, 60°; taper ratio, 0.25; Mach number, 1.5.

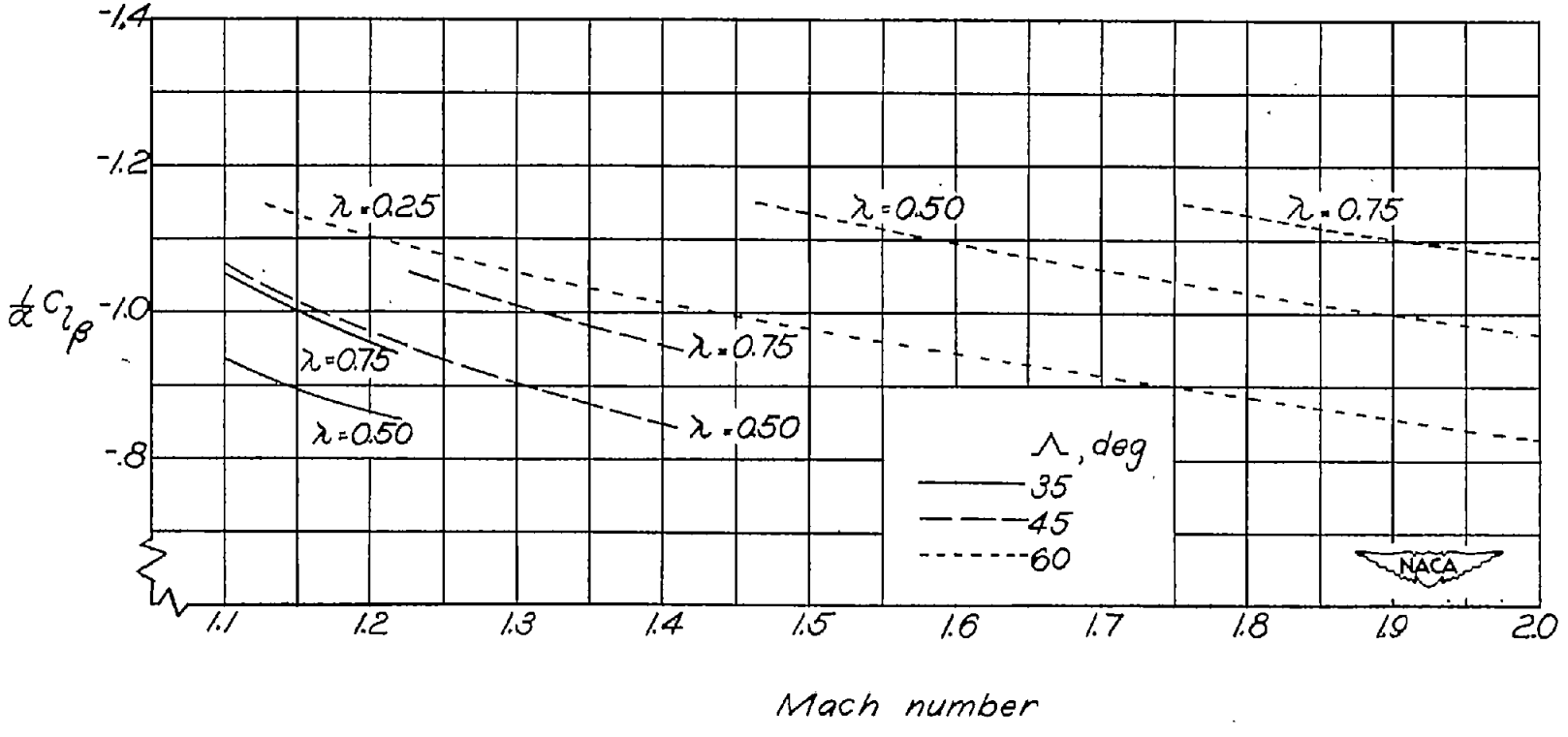

Figure 12.- Variation of the stability derivative C_{l_β} with Mach number for various wings of aspect ratio 2. (All angles measured in radians; results are valid for both body and stability systems of axes.)

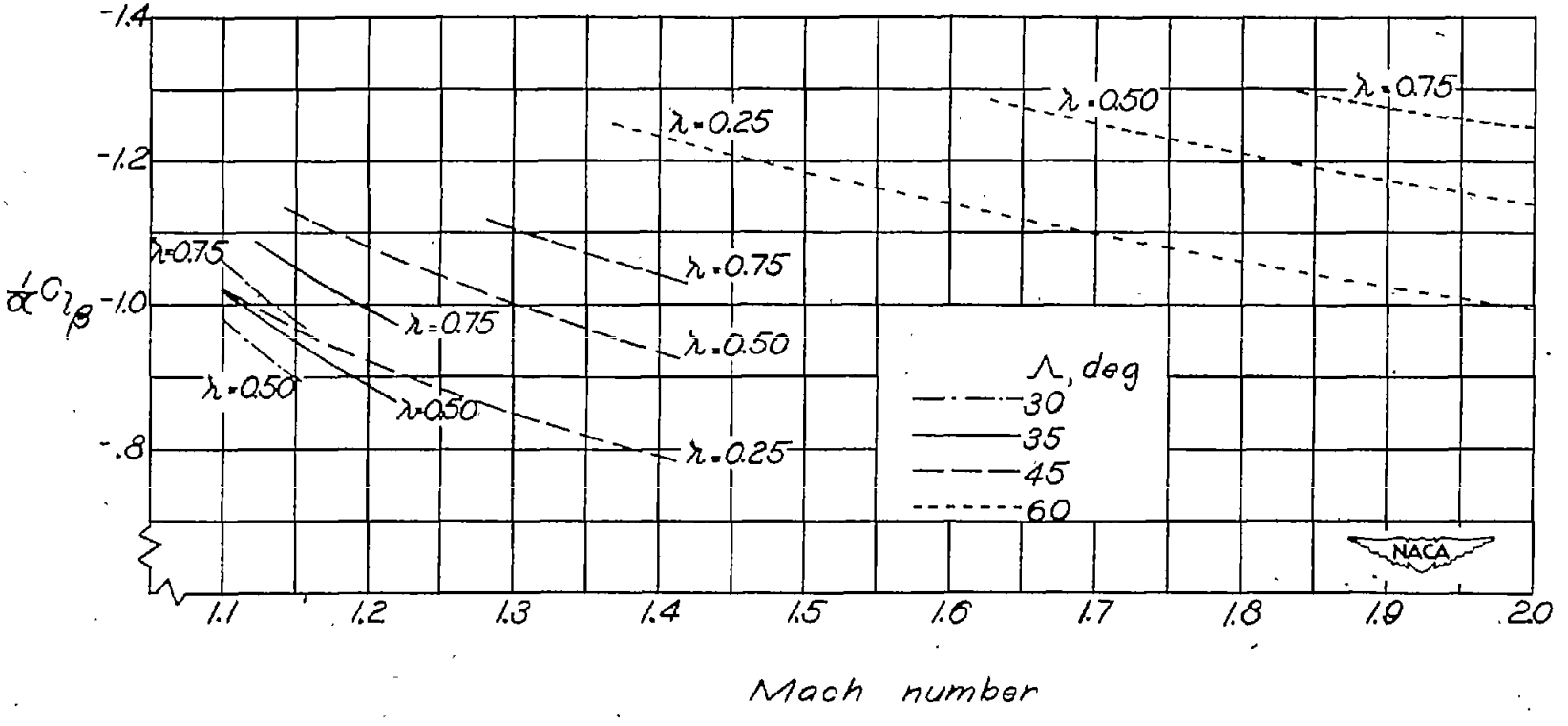

Figure 13.- Variation of the stability derivative C_{l_β} with Mach number for various wings of aspect ratio 3. (All angles measured in radians; results are valid for both body and stability systems of axes.)

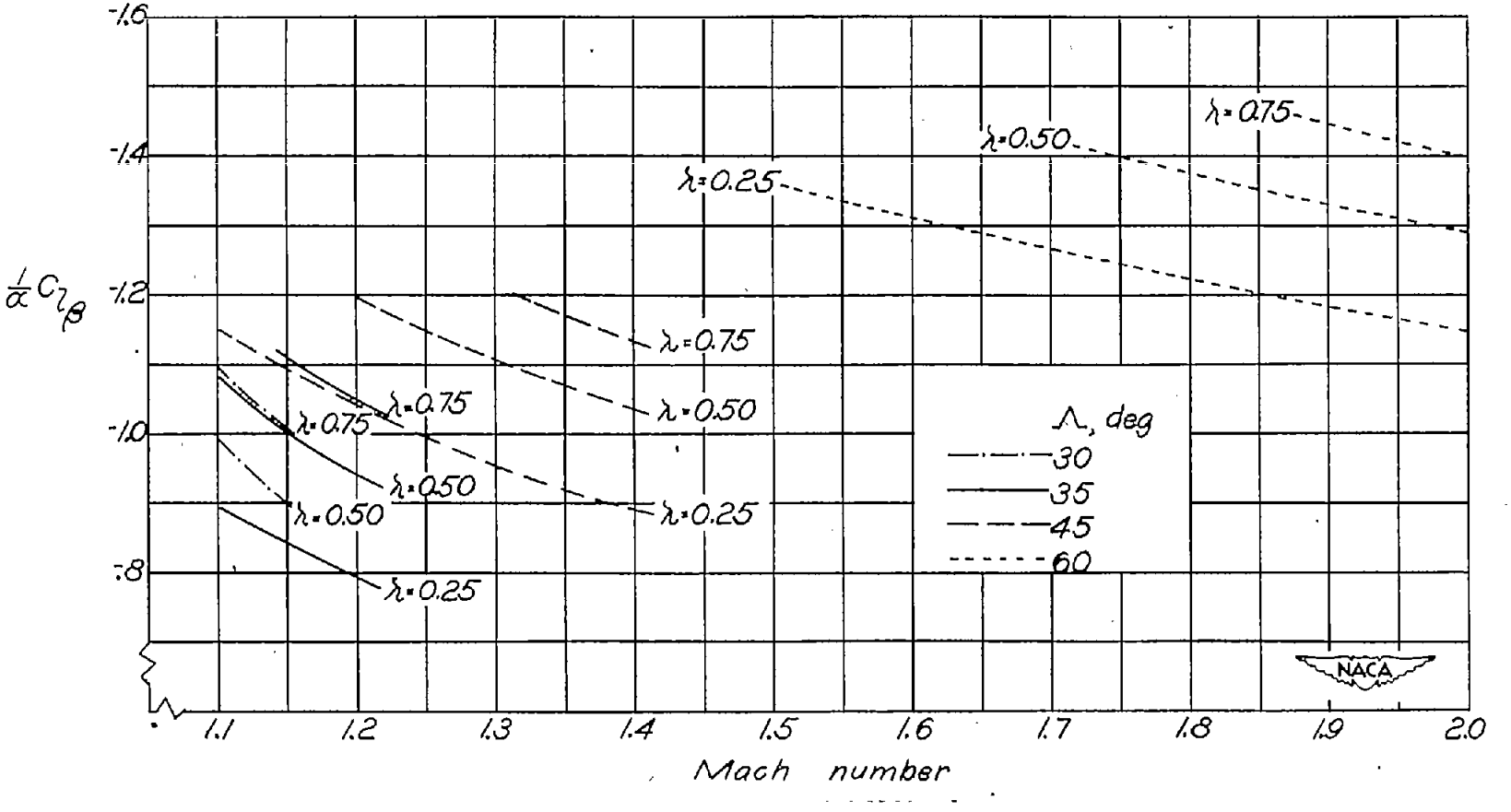

Figure 14.- Variation of the stability derivative C_{l_β} with Mach number for various wings of aspect ratio 4. (All angles measured in radians; results are valid for both body and stability systems of axes.)

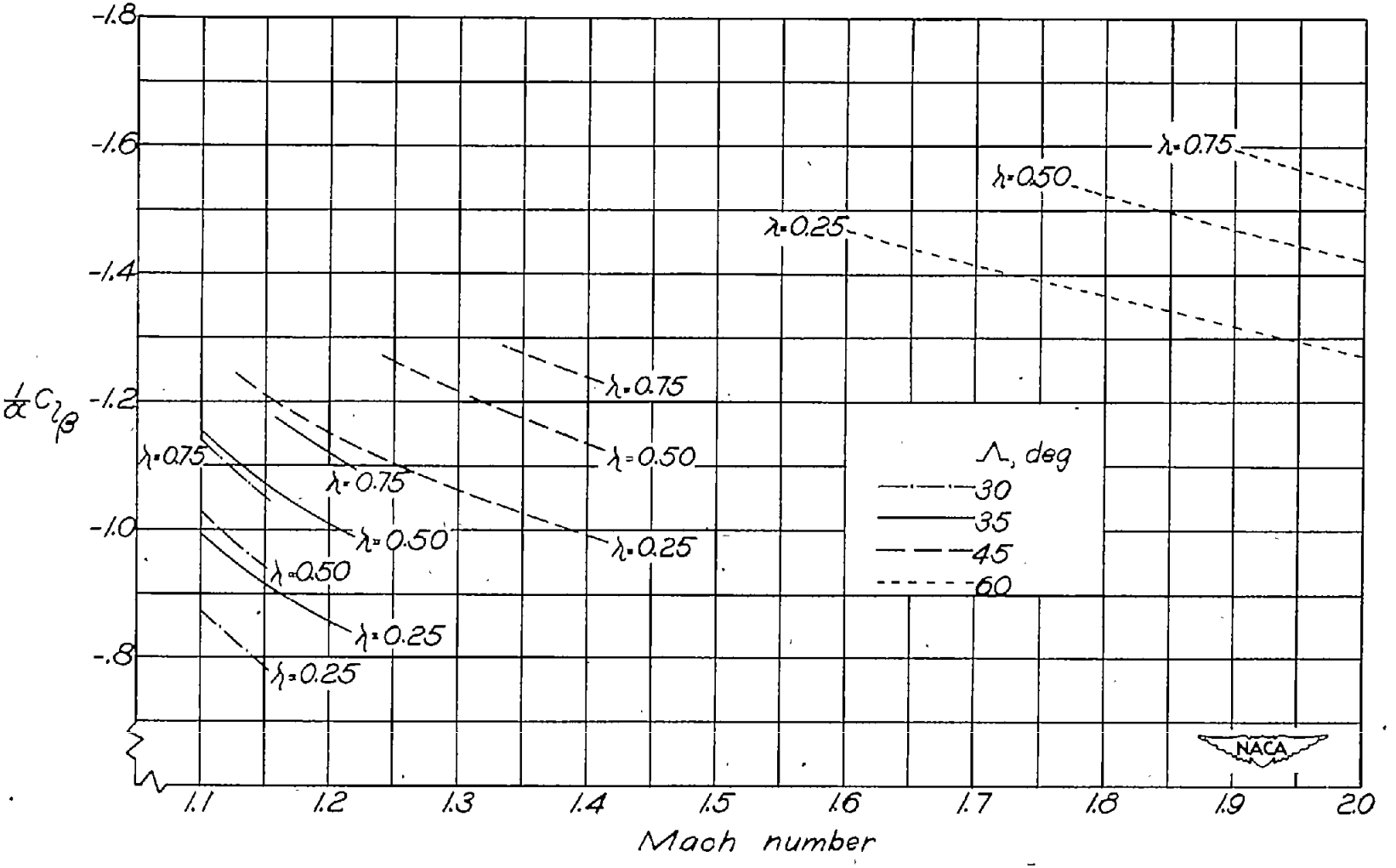

Figure 15.- Variation of the stability derivative C_{l_β} with Mach number for various wings of aspect ratio 5. (All angles measured in radians; results are valid for both body and stability systems of axes.)

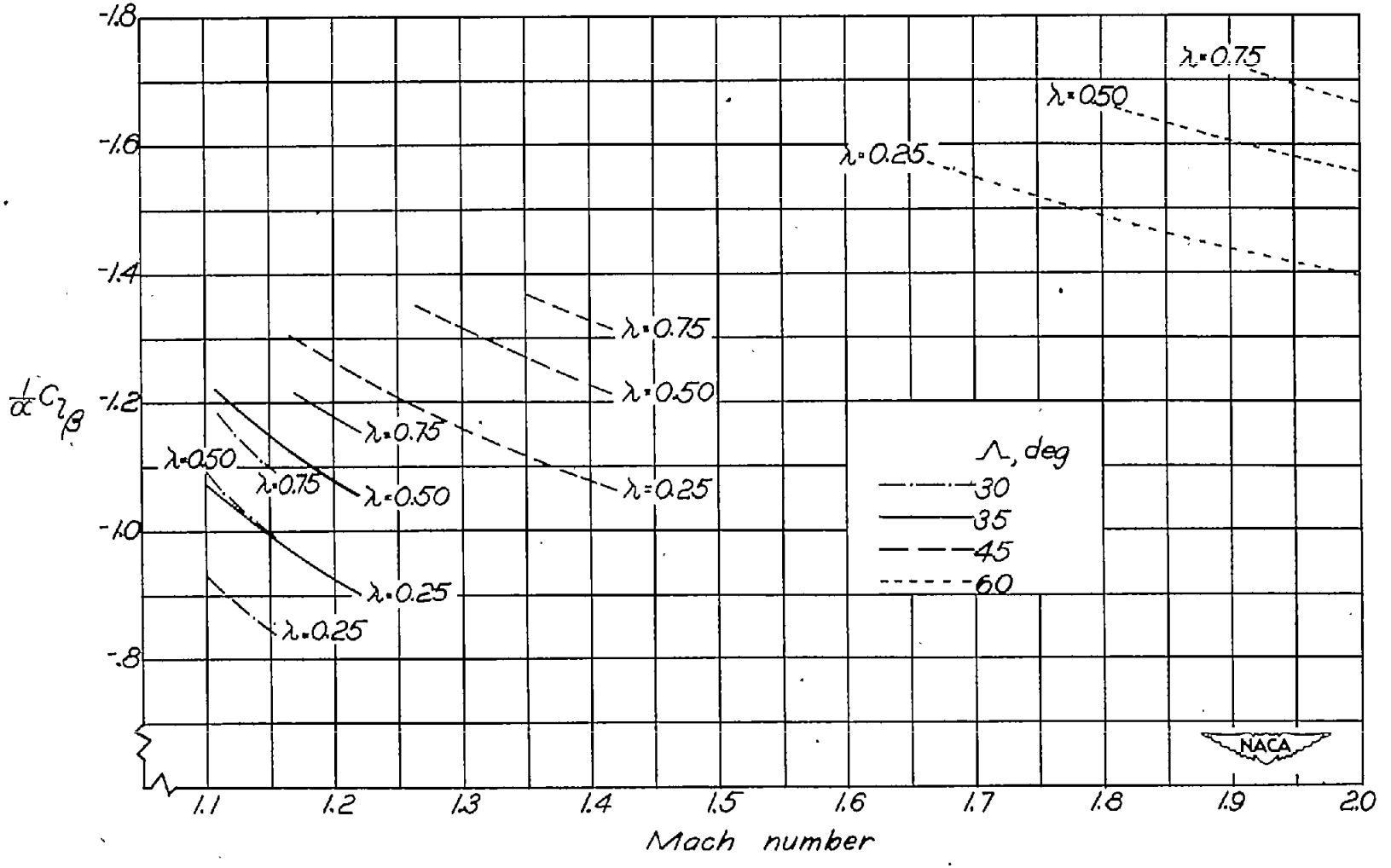

Figure 16.- Variation of the stability derivative C_{l_β} with Mach number for various wings of aspect ratio 6. (All angles measured in radians; results are valid for both body and stability systems of axes.)

NACA-Langley - 3-27-53 - 1000